In-field measurement and numerical modelling of air leakage in concrete: From laboratory specimen to structural full-scale

S. Multon, Donatien Rossat, Jerome Verdier, David Bouhjiti, Hognon Sogbossi, Julien Baroth, Ali Nehme, Frédéric Dufour, Hugo Gérard Jacques Cagnon, Matthieu Briffaut

In-field measurement and numerical modelling of air leakage in concrete: from laboratory specimen to structural full-scale

S. Multon[1,*], D. Rossat[2], J. Verdier[1], D. Bouhjiti[3], H. Sogbossi[1], J. Baroth[2], A. Nehme[1], F. Dufour[2], H. Cagnon[1], M. Briffaut[2]

[1] *Université de Toulouse; UPS, INSA; LMDC (Laboratoire Matériaux et Durabilité des Constructions); 135, avenue de Rangueil; F-31 077 Toulouse Cedex 04, France*

[2] *Univ. Grenoble Alpes, CNRS, Grenoble INP, 3SR, F-38000 Grenoble, France*

[3] *IRSN, PSN-EXP/SES/LMAPS, F-92262 Fontenay aux Roses, France*

Abstract

This work estimates air leakage through concrete porosity for structures by using data obtained in field combined with stochastic finite element (SFE) modelling. For this purpose, a methodology is proposed to evaluate permeability under representative over-pressurization conditions based on in-field measurements under vacuum. This makes it possible to investigate the air leakage through the inner wall of a 1:3 scaled nuclear vessel named the VeRCoRs mock-up. Measurements are made for over 80 points scattered on the external face of the inner wall of the structure. Based on the data collected, a statistical analysis quantifies the spatial variation of permeability and contributes to the building of an SFE model of air leakage at the structural scale. Measured and predicted data are in good agreement on the service life of the structure. This shows the relevance of combining in-field measurements during an operational phase and the SFE modelling for better evaluation of the structural performance. The lessons learnt from the present work could be useful for the assessment of all structures with durability or mechanical issues that induce a continuous loss of tightness.

Keywords

Air leakage, concrete structures, permeability measurement, stochastic analysis, VeRCoRs mock-up.

[*] Corresponding author, *e-mail address: Stéphane Multon, multon@insa-toulouse.fr*

1 Introduction

The durability of concrete is a major issue in the management of civil engineering structures and induces the need for continuous monitoring of their behaviour to ensure the safety of both the structure and the surrounding environment. The dimensions of large structures (which can reach 1 metre in thickness and several dozens of metres in length in certain strategic structures), the presence of reinforcement and, possibly, of prestressing cables, make the in-depth evaluation of concrete properties over time difficult; especially when only non-destructive techniques can be used.

Much research is currently taking place on this topic as such techniques appear promising. In the case of nuclear vessels, the concrete constituting the confinement enclosures must have low transport properties to guarantee the tightness of the walls and to prevent the release of radioactive products into the environment throughout its lifetime. The permeability test provides a reliable and fast quantification of gas transport for such applications, and regular measurements must be made throughout the service life of these structures. Local permeability measurements are complementary to the usual pressurization tests where the main goal is to measure the global tightness to prevent any excessive leakage. However, the reliable quantification of such local quantities remains a challenge because of the large external surface area (need for numerous measurements), the thickness (difficulty of measuring permeability in the wall core) and, predominantly, the natural variability of the properties of concrete. Hence, when such large structures are assessed, the use of mean values of properties is not sufficient; a stochastic approach is of great interest.

The present paper focuses on the evaluation of air leakage through concrete in structures representative of nuclear vessels by using testing techniques coupled with stochastic Finite Element (FE) modelling. From the experimental point of view, the Cembureau test is the laboratory technique most commonly used on small specimens to measure their air permeability under pressure [1]. It cannot be used for in-field measurement unless it is performed on cores drilled from the structures, which is not possible in the case of operating nuclear vessels. Different techniques (mostly vacuum techniques) currently exist for in-field measurements of air permeability [2–8].

The first part of this paper is dedicated to the research significance to underline the scientific issues concerning the measurement of air permeability in field and the stochastic evaluation of the leakage rate of the VeRCoRs mock-up[1] [9,10]. In the second part, the concrete mix-designs are described. In the third par, the method to evaluate the permeability under pressure based on in-field measurements under vacuum is presented. The fourth part deals with an experimental investigation of the mock-up using the previous technique. Measurements are made at 80 points scattered on the external side of the reinforced wall of a mock-up representative of containment vessels. At the structural scale, the transport properties of the wall are assumed to be the same, except for the natural dispersion of the building material. Based on the data collected, statistical analyses are performed to quantify the spatial variation of permeability at the structural scale. The fifth and last part presents a stochastic FE model of the air leakage in VeRCoRs. The numerical results in terms of global air leakage are compared with the results observed during the pressurization tests.

2 Research significance

In the field, the main obstacles to performing relevant measurements of concrete air-permeability are the difficulty of controlling the air flow in the structure (and thus the geometry of the concrete volume investigated) and the type of flow regime. Due to the large size of most concrete structures, e.g., the thickness of the inner wall of a nuclear containment building

[1] The VeRCoRs mock-up is a 1:3 scaled nuclear containment building and a research programme aiming to better understand the long-term behaviour of Nuclear Power Plants

(NCB), which is about 1 m, no in-field techniques can guarantee a truly steady state measurement and a unidirectional flow as in laboratory conditions.

Technical solutions were proposed in the literature to evaluate the air permeability in field [2–6,8,11]. To control the air flow, Torrent proposed a vacuum technique (*Figure 1*) based on the complementarity of two cylindrical cells ([2] – *Figure 2*). During a first stage, the two cells were subjected to a vacuum for 60 seconds (*Figure 2*). During the second stage, the vacuum was no longer imposed. Due to the pressure difference, air flowed from the concrete towards the central cell. The pressure in the cell increased and Torrent has proposed an evaluation of the permeability from the pressure increase measured in the central cell during less than 15 minutes. At this stage, the pressure in the external cell was equal to the pressure in the central cell thanks to the use of a pressure regulator [2]. As the pressure was the same in the two cells, the air flow was controlled [2].

Figure 1: Torrent device for permeability measurement (acquisition system, pump and Torrent's cell on a laboratory sample)

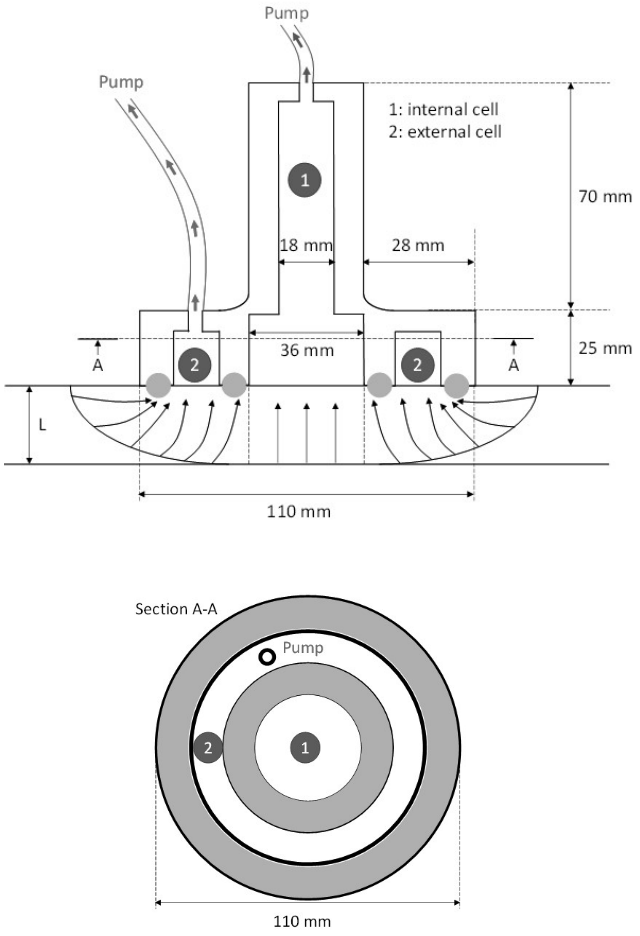

Figure 2: Pictorial representation of Torrent device for permeability measurement

It was first necessary to compare measurements under pressure and in vacuum. This comparison has been made on laboratory samples for steady state and unsteady state in [7,12]. The mean free paths of gas molecules are greater in vacuum than in overpressure. However, the use of Klinkenberg theory [7,12,13] made it possible to evaluate the air permeability under pressure from permeability evaluated in vacuum.

The objectives of the work presented here were to apply the methodology previously presented for small laboratory samples (50 mm thick) in [12], to in-field measurements made on the wall of the VeRCoRs mock-up and to provide input data to a stochastic FE model of air leakage evaluation. VeRCoRs has been specifically designed to study the safety and ageing of containment walls, with particular emphasis on predicting the leakage rate [10]. Several numerical studies have been performed to evaluate the mechanical behaviour, with a particular focus on cracking, and the leakage rate at different times of the mock-up [14–17]. In these studies, the numerical work was mainly focused on the leakage through cracks [15]. In [17], special attention was given to the porosity leakage (air leakage through concrete porosity). But because of the lack of data, the permeability was chosen after literature review [17,18]. The present study focused mainly on the porosity leakage, which is an important contributor to the total leakage of the structures. The aim was, first, to use the permeability data measured in situ to refine the prediction of the porosity leakage with data obtained on the concrete used in field. Furthermore, the stochastic approach allows the description of the variability of the permeability field of the structure in a probabilistic setting. In this context, the proposed model can predict the leakage rate of the structure with the associated uncertainties, which has never been done before. Several random variables, e.g. the hydric diffusivity for drying, the initial water content in the concrete, the air permeability and its pressure dependence, impact the modelling of the physical problem. In this study, the spatial variability of the permeability is evaluated from measurements in situ whereas the variability of the other input is considered as uniform in the structure. Finally, the leakage predictions based on this probabilistic approach are compared with in situ measurements of the leakage rate of the structure during pressurization tests.

3 Material characterization

The laboratory experimental work was performed with three concrete mix-designs, referenced as C1, C2 and C3, representative of a wide range of usual concrete based on Portland cement (**Table 1**). Three water/cement (W/C) ratios between 0.4 and 0.55 (Table 1) were used to obtain a range of accessible porosity between 14% and 18% (**Table 2**). Water porosity was measured between total saturation of the sample with water after exposure to vacuum and drying at 105

°C. The usual trend of porosity was obtained: increase in water porosity with increase in W/C ratio.

The study focused mainly on the characterization of the concrete C2. It was representative of the VeRCoRs mock-up and was the subject of a larger project [19]. Several batches of this concrete were produced during the course of the project. The two other concrete mixes (C1 and C3) were cast specifically for this study, and only one batch was produced. Permeability measurements were evaluated on two batches of concrete C2, referenced as C2-B1 and C2-B2. To stabilize the cement hydration, specimens were cured in lime water at a temperature of 20 ± 2 °C for about 60 days after casting [20]. The properties of the four concrete batches of the three mix-designs after the curing period are given in **Table 2**. After 60 days in limewater, the hydration of CEM I cement is usually stabilized [20]. Therefore, the evolutions of the mechanical and air permeability after 60 days should be therefore limited [21–24].

Table 1. Concrete mixes

Constituents [kg/m^3]	**C1**	**C2**	**C3**
Sand 0/4	941	830	858
Gravel 4/11 R	-	445	-
Gravel 8/16 R	-	550	-
Gravel 4/12.5 R	1020	-	945
Cement CEM I 52.5 NCE CP2 NF	280	320	400
Plasticizer	2	2.4	3
Efficient water	155	167	171

Table 2. Concrete properties

	C1	C2-B1	C2-B2	C3
Water porosity (%)	18	16.7	15.2	14
Young's modulus (MPa)	31700	32300	39200	38800
Compressive strength* (MPa)	40.2	41	46.8	57.8

*Uniaxial compressive strength after 28 days

Experiments were performed on usual laboratory samples for Young's modulus and compressive strength (110 mm diameter and 220 m height) and permeability measurement (150 mm diameter and 50 mm thickness).

The objective of the experimental work was to verify the ability of the proposed approach to evaluate the permeability property under pressure from the measurement under vacuum. To evaluate the method, it was important to test it on materials with various porosity values. Thus, the permeability was measured with the different methods on samples with saturation degrees, between 3% and 70%. The accessible porosity ranged from 5 to 18%. The saturation ratio of all the specimens was controlled by the following conditioning to limit thermo-hydric gradients and resulting skin cracking [25–27]:

1. Saturation: Specimens were water saturated under vacuum,
2. Drying: Specimens were dried with an increasing drying temperature (40 °C to obtain a saturation of 80%; 50 °C to obtain saturation levels of 60, 30 and 10%; 80 °C to obtain a saturation of 3%; and 105 °C to obtain the driest state in this study, corresponding to zero saturation). Targeted masses were evaluated from the porosity measured on other samples cast with the same batch of concrete.
3. Homogenization: Specimens were placed in sealed conditions (aluminium and sealed bags) once the target mass had been reached and put back into the oven (for a minimal duration equal to the drying time in order to slightly homogenize the water distribution throughout the sample).

The saturation levels representative of the real structure are between 30 and 80%. In the laboratory, these saturation levels were all obtained with a drying temperature lower than 50 °C to avoid the modification of the cement hydrates and the development of drying cracks. All the calculations made for the mock-up in this paper were based on these representative values. Drying at 80 °C and 150 °C was performed only to have common reference values for porosity and permeability measurements. The smallest saturation ratio obtained after a 105 °C drying process was taken to be 0% of saturation in this work.

4 Experimental methodology

The objective of this section is to propose an evaluation of intrinsic permeability (permeability corresponding to viscous flow and assumed to be independent of fluid and test conditions) and to quantify the dependence of air permeability to pressure from permeability measurement in vacuum. The technique of in-field measurement of permeability was first evaluated in the laboratory and compared to the standardized technique for permeability measurement.

4.1 Experimental techniques for in-field permeability measurement

4.1.1 Evaluation of the air permeability by means of an increase of pressure after vacuum

In their experimental works of 1995, Yssorches et al. [28] used a permeability measurement based on a vacuum technique. During the measurement, a vacuum was imposed on one face of a concrete sample for a certain time (0 or 2 hours), then the permeability was evaluated from the pressure increase when the pumping was stopped [28]. This technique was used for samples with small thickness and the direction of the air flow was controlled by an external seal. The permeability evaluated in the first stage of the pressure increase was not representative of the real permeability [28]. The authors showed that, for small samples in the laboratory, the increase became almost linear after a long period of time (at least 15 minutes). They recommend that permeability should be evaluated from the slope of the increase when the regime is stabilized. For small samples, stabilization is obtained when the air flow crosses the thickness completely. As the pressure was not maintained constant, the flow was never perfectly constant: the pressure profile in the thickness of the sample was never perfectly stabilized (but the variation with time became small) and the regime was pseudo-steady [28].

At the beginning of the pressure increase, the regime seems to be disturbed by the modification of the boundary conditions, particularly for a small duration of vacuum [28]. The sudden stopping of the pumping and the moisture gradient in the concrete skin may be responsible for this effect. As the first centimetres of concrete are usually dryer than in depth, the depth investigated increases fast at the beginning of the pressure increase (occurring in dry concrete) and slows down when the air flow reaches deeper concrete with a higher saturation ratio. Therefore, the interpretation of the pressure increase in the central cell of Torrent's apparatus has been analysed based on the conclusions obtained in [28]. Once the pseudo-steady regime is obtained in the central cell, the apparent permeability (in fine concrete porosity, air flow depends on pressure because of the slip effect on pore wall due to molecular contribution – apparent permeability is thus equal to the sum of viscous and slip flows [29]) and can be deduced from the Hagen-Poiseuille equation and from the conservation of the air mass between the concrete porosity and the volume of the cell [13,30]:

$$k_{a_{psr}} = \frac{2 \cdot \mu \cdot L}{A \cdot (P_{atm}^2 - P_c^2)} \cdot V_c \cdot \dot{P}_c \qquad \textit{Eq. 1}$$

with $k_{a_{psr}}$ the apparent permeability obtained during the pseudo-steady regime, μ the air viscosity, L and A the thickness and the cross-section of the sample, respectively, P_{atm} the atmospheric pressure, V_c the volume of the cell, P_c the pressure in the cell and $\dot{P}_c$ the initial slope of the pressure increase in the cell.

In the work presented here, the saturation ratio, the accessible porosity and the apparent permeability are considered constant and homogenous in the depth investigated, as is usual for such measurements.

Due to the large thickness of the walls of real structures, and particularly for vessels of nuclear plants, the vacuum time needed is too long for permeability measurement to be performed in such controlled conditions. The main difficulty is then to evaluate the depth of concrete impacted by the air flow. In his approach, Torrent proposed an evaluation of this depth, L_0, from the mass balance of air moles crossing the concrete to reach the central cell during the test [2]:

$$L_0 = \sqrt{\frac{2 \cdot k_{a_t} \cdot P_{atm} \cdot (t_v + t)}{\varphi \cdot \mu}} \qquad \textit{Eq. 2}$$

with: k_{a_t} the unknown permeability of concrete crossed by the air flow, t_v the vacuum time, t the time after the pumping was stopped, φ the porosity of concrete, and μ the air viscosity.

The combination of the two previous equations enables the permeability, k_{a_t}, to be evaluated from the evolution of the pressure in the central cell for any time, t, by the following equation:

$$k_{a_t} = \frac{8 \cdot \mu}{\varphi} \cdot \left(\frac{V_c}{A}\right)^2 \cdot \frac{P_{atm}}{(P_{atm}^2 - P_c^2)^2} \cdot \dot{P_c}^2 \cdot (t_v + t) \qquad \textit{Eq. 3}$$

The air flow rapidly becomes almost constant across the concrete (pseudo-steady state) for specimens with small thickness and large permeability. The permeability can thus be evaluated. For intermediate permeability, the air flow can cross the thickness (only the external surface is at atmospheric pressure), but the duration of the pressure increase is too small for the pseudo-steady state to be reached. For such short times, the permeability should be evaluated by Eq. 1. but an overestimation of the permeability is probable [28]. For specimens with same thickness and lower permeability, the air flow does not cross the thickness (part of the concrete inside the sample is still at atmospheric pressure). Eq. 3 should be used to calculate the permeability.

With Eq. 3, the evaluation of the permeability is based on the evaluation of the depth, L_0, (Eq. 2) of the concrete investigated. The evaluation of L_0 depends on the concrete accessible porosity [2]. The accessible porosity for air molecules in the field depends on the concrete saturation ratio and the accuracy of the permeability measurement depends on the accuracy of the concrete porosity estimation. Various non-destructive methods have been proposed to evaluate the concrete saturation ratio [31–34]. For the evaluation of L_0, the linearity of pressure is assumed through a certain depth of concrete [2]. The profile is not really linear along this depth and this can lead to an incorrect estimation of the permeability. To improve the technique, it is important to evaluate the time for which the evaluation of L_0 is the most relevant, for small, average or long durations of pressure increase.

4.1.2 Application

This determination of the permeability measured under vacuum was applied to three samples of the three mix-designs presented above (Tables 1-2) for different saturation ratios (Figure 3). The pressure increase with time of the sample C2 (batch B2), obtained with Torrent's apparatus ([2] – Figure 1), is shown in Figure 3 for three saturation ratios (65, 33 and 10%).

The apparatus is automated to stop the pressure increase after a variation of about 20 mbars, or after 660 seconds (Figure 3). The slope was evaluated for the last two minutes of the increase. From the slope given by the pressure increase recorded by Torrent's apparatus, it is possible to evaluate the concrete permeability in vacuum conditions: using Eq. 1 if the sample is crossed by the air flow, or by using Eq. 3 if the air flow does not reach the other side of the sample. This is determined from Eq. 2. If L_0 is less than 50 mm, then k_{a_t} is the permeability under vacuum. If L_0 is more than 50 mm, then $k_{a_{psr}}$ is the permeability under vacuum. For the three concrete mix-designs, most of the samples with saturation ratios lower than or equal to 30% were crossed by the air flow. Most of the other samples were not crossed.

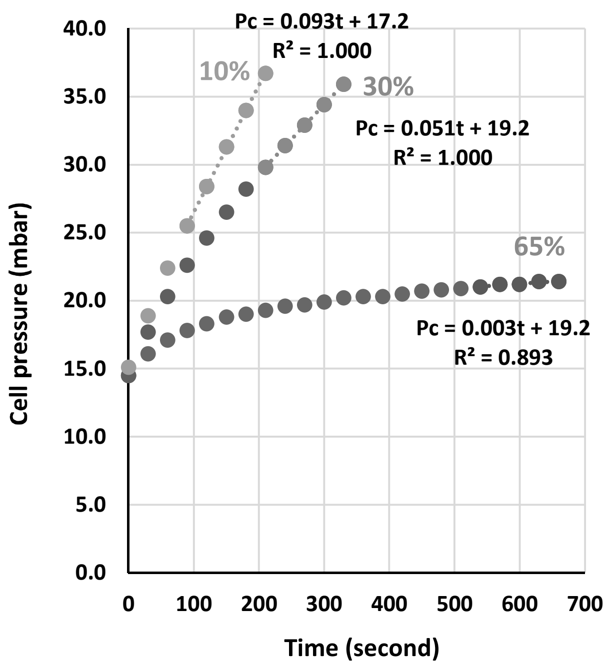

Figure 3: Increase of pressure in the central cell of the apparatus and determination of the slope for evaluation of the permeability of a given sample at 3 different saturation ratios (10, 30 and 65%)

The apparent permeability obtained for the three concrete mix-designs at the different saturation ratios is shown in Figure 4. As expected, the permeability changes significantly for small variations of saturation ratios above 60% [35].

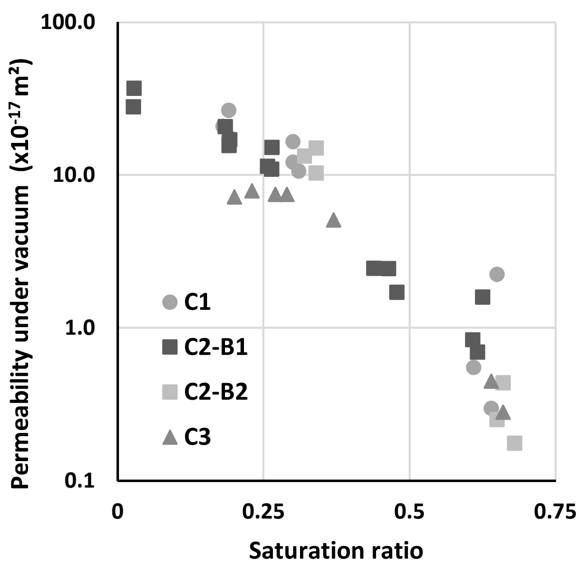

Figure 4 : Apparent permeability obtained under vacuum according to the saturation ratio (logarithmic vertical axis)

4.2 Comparison with Cembureau technique

4.2.1 Cembureau permeability as a reference for the permeability measurement

The objective of this work was to evaluate the intrinsic permeability, denoted k_i, and usually evaluated under pressure, from the permeability under vacuum. For this purpose, the concrete permeability evaluated with the Cembureau technique was defined as the reference permeability ([1] – Figure 5). Permeability measurement with the Cembureau technique is based on the steady state measurement of a unidirectional air flow crossing the cross-section of a sample subjected to a constant pressure gradient lying usually between 1 and 4 bar.

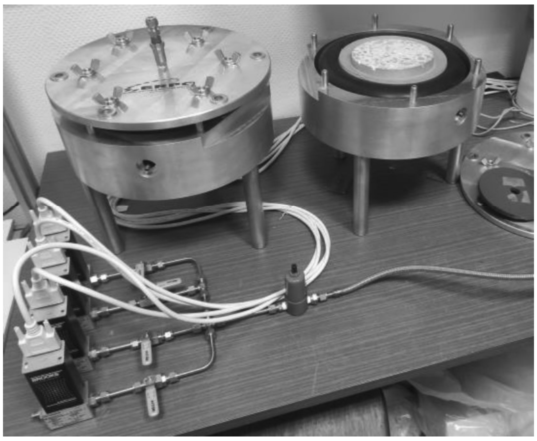

Figure 5: Cembureau device for permeability measurement in laboratory

For each sample, the apparent permeability under pressure was evaluated at 4 pressure levels by applying 2, 3, 4 and 5 (or 6) bars to one face of the sample while the other face was under atmospheric pressure. The relationship between the apparent permeability and the reciprocal of the mean pressure of the test is linear. This relationship is commonly referred to as Klinkenberg's law. Intrinsic permeability (ordinate to the origin of this line) and the slope were evaluated for every sample and every saturation ratio. The values for a sample of concrete C2-B1 at 4 saturation ratios are shown in Figure 6.

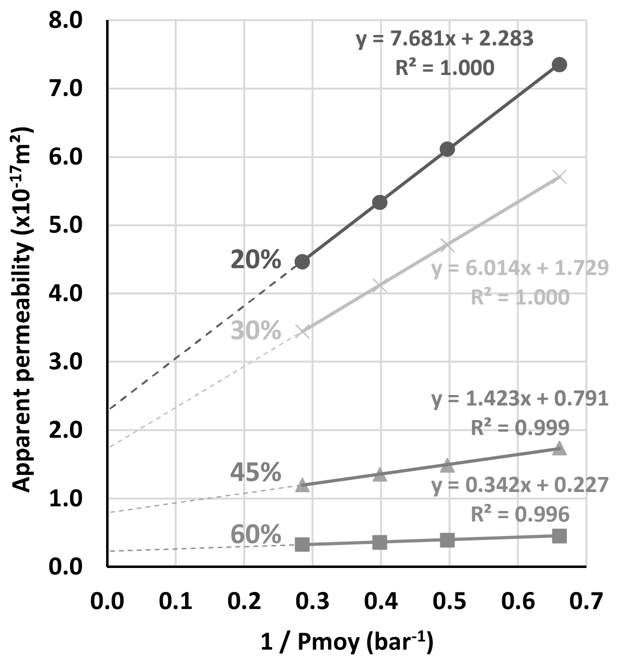

Figure 6: Apparent permeability versus the inverse of the mean pressure for Cembureau tests performed on a single sample at 4 different saturation ratios (20, 30, 45 and 60%)

These tests were performed on all the samples of the experimental programme with a focus on usual in situ saturation ratios in concrete, i.e. between 20 and 80%. Above 70-80% of saturation, the three concretes were air-tight (see Figure 7). At 60%, the concrete C1 showed the greatest permeability. At 30%, the differences in permeability were small and close to the usual scatter found on permeability measurements. However, the permeability trend for the three mixes was similar to the water porosity trend: permeability increased with increasing W/C ratio (Figure 6). Under 20% saturation, concrete samples were exposed to 80 °C. This led to significant thermo-hydric damage [36]. It increased permeability discrepancy (Figure 7) and the concrete was no longer representative of usual exposure conditions of structures. It was only performed for one concrete in this study (Figure 7).

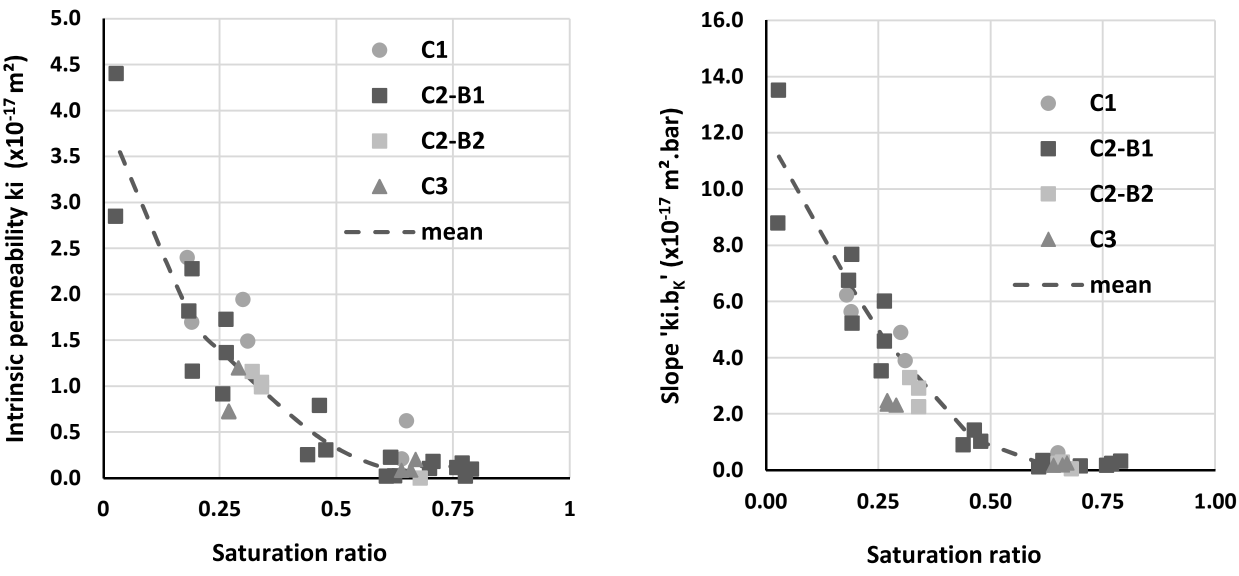

(a) (b)

Figure 7: Reference intrinsic permeability (a) and reference slope of Klinkenberg's law (b) versus saturation ratio for the three concretes

4.2.2 Determination of the intrinsic permeability from a single permeability measurement

To be able to evaluate the air leakage of a structure under pressure, it is necessary to determine both the intrinsic permeability and the slope of Klinkenberg's law [29]:

$$k_a = k_i\left(1 + \frac{b_k}{P_m}\right) \qquad \textit{Eq. 4}$$

with k_a the apparent permeability, k_i the intrinsic permeability, P_m the mean pressure between the atmospheric pressure and the pressure of the test, and b_k, the Klinkenberg gas slippage factor.

Apparent permeability measured in vacuum for different pressures is close to the prolongation of Klinkenberg's law for the domain of pressure lower than atmospheric pressure [12,13]. However, the slope of the variation of the apparent permeability with pressure for measurements in vacuum does not correspond to the slope of Klinkenberg's law [12]. It is thus not possible to evaluate the slope by measuring permeability with different input pressures in vacuum. Sogbossi et al. [12] proposed an evaluation of the intrinsic permeability from a single permeability measurement (under pressure or in vacuum) based on theoretical and empirical concepts [13,29,37]. From Klinkenberg's theory [29], the following relationship has been established:

$$k_{a_2} = C_P k_{a_P} \qquad \textit{Eq. 5}$$

with k_{a_2} the apparent permeability for an absolute pressure of 2 bars, and k_{a_P} the apparent pressure for any pressure P. C_P is a function of the pressure and of the pore network. Many authors have shown the relation between the apparent permeability and the characteristic dimensions of the pore network of porous media [13,38–45]. Permeability could thus be evaluated from the pore size distribution obtained by Mercury Intrusion Porosimetry [43]. Sogbossi's PhD thesis [13] proposed the evaluation of C_P, linking the apparent permeability at different pressures, as a mean value calculated for the smallest pores of the network lying between a minimal value R_0 and a maximal value R_1 [12,37]:

$$C_P = \overline{C_P} = \frac{1}{R_1 - R_0}\int_{R_0}^{R_1}\left(\frac{r + 0.171}{r + 0.268/P_m}\right)dr \qquad \textit{Eq. 6}$$

with P_m the real mean pressure between the atmospheric pressure and the pressure of the test, P, taking the compressibility of air into account [12]. In Sogbossi's work, the values of radii were calibrated to obtain a correct evaluation of apparent permeability in vacuum from a measurement under pressure in the steady state.

The result of this integral is:

$$\overline{C_P} = 1 + \frac{0.171 - \frac{0.268}{P_m}}{R_1 - R_0} ln\left(\frac{R_1 + 0.268/P_m}{R_0 + 0.268/P_m}\right) \qquad \textit{Eq. 7}$$

Thus, the intrinsic permeability and the slope of Klinkenberg's law can be evaluated from only one permeability measurement under pressure or in vacuum.

In the present work, this approach is first validated for the three concretes of the study under pressure. Combining Eq. 4 and Eq. 5, the slope can be estimated with the Cembureau technique from the apparent permeability measured for an absolute pressure of 2 bars:

$$b_k k_i = k_{a_2} \frac{1 - \frac{1}{\overline{C_5}}}{\frac{1}{P_{m2}} - \frac{1}{P_{m5}}} \qquad \textit{Eq. 8}$$

where P_{m2} is the real mean pressure between the atmospheric pressure and 2 bars, and P_{m5} the mean pressure between the atmospheric pressure and 5 bars. The intrinsic permeability can then be calculated as:

$$k_i = k_{a_2} - \frac{b_k k_i}{P_{m2}} \qquad \textit{Eq. 9}$$

The two equations are valid for absolute pressures lower than 0.5 bar and higher than 2 bars. In Figure 8, the results obtained with these equations are compared to the reference slope and to the intrinsic permeability experimentally determined in the previous part. In the present work, the maximal pore radius, $R_{1,}$ was calibrated to obtain good correspondence for the three concretes and for saturation ratios between 20 and 70%, with a maximal pore radius, $R_{1,}$ of 0.2 µm (the minimal value, R_0, was taken to be equal to 0.01 µm as proposed in Sogbossi's work [12]). For such radii, the quantity $\overline{C_5}$ is equal to 1.58, which is consistent with the results obtained during the development of the methodology [13]. The order of magnitude of this maximal pore radius is consistent with radius size considered in previous numerical studies on air permeability in concrete [43–45].

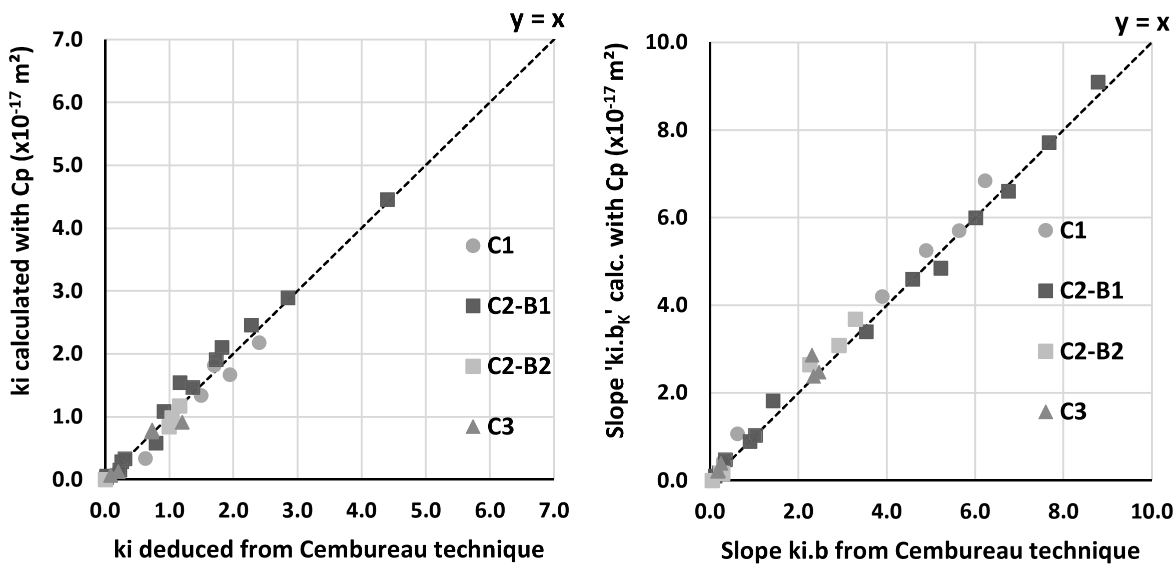

(a) (b)

Figure 8: Comparison between the intrinsic permeability (a) and the slope of Klinkenberg's law (b) obtained by Cembureau technique and the values deduced from the apparent permeability at 2 bars and C5 equal to 1.58 (maximal radius of 0.2 µm)

4.2.3 Comparison between the intrinsic permeability evaluated in vacuum and the intrinsic permeability evaluated under pressure

As explained above, vacuum techniques are very interesting to evaluate the permeability of real structures. As the intrinsic permeability and the slope of Klinkenberg's law cannot be evaluated directly from different apparent permeability values obtained in vacuum [12], the methodology presented just above was used. In this case, only an apparent permeability in vacuum, k_{a_v}, is known. The slope and the intrinsic permeability were obtained by combining Eq. 5, Eq. 8 and Eq. 9:

$$b_k k_i = C_v k_{a_v} \frac{1 - \frac{1}{C_5}}{\frac{1}{P_{m2}} - \frac{1}{P_{m5}}} \qquad \text{Eq. 10}$$

and

$$k_i = C_v k_{a_v} - \frac{b_k k_i}{P_{m2}} \qquad \text{Eq. 11}$$

C_v was determined from Eq. 7 with the same maximal radius of 0.2 µm evaluated in the previous part and from the pressure measured by the central cell of the vacuum apparatus. In this situation, C_v was about 0.545, in agreement with the previous work [13].

In Figure 6, the intrinsic permeability and the slope evaluated from the apparent permeability measured under vacuum (presented in Figure 4) are compared to the reference values for the intrinsic permeability and the slope determined with the Cembureau technique. This method led to an overestimation of both the intrinsic permeability and the slope, by about 60%. This result can be partly explained by the presence of parasitic fluxes on the thin samples tested, due to the geometry of the system. It is important to note that this overestimation was quite similar for the three Portland concretes used in this experimental study and could thus be extrapolated to the in-field concrete investigated in the following part.

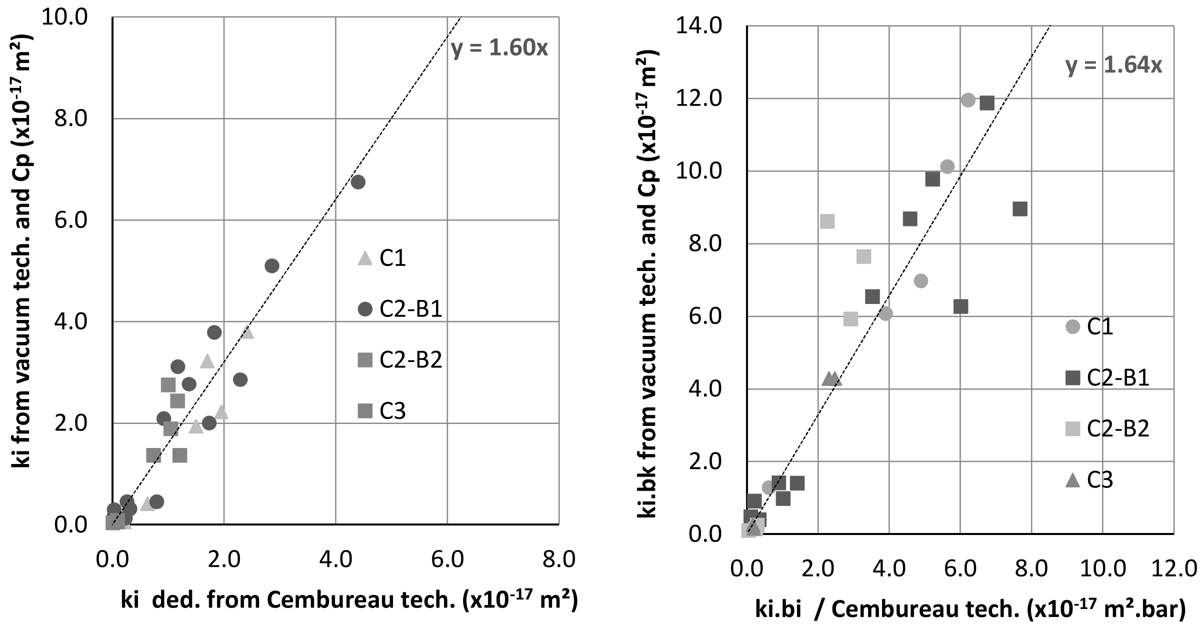

(a) (b)

Figure 9: Comparison between the intrinsic permeability (a) and the slope of Klinkenberg's law (b), obtained by the Cembureau technique, and the values deduced from the vacuum permeability and Cp, for Cp equal to 0.545

The experiments presented here showed that it is possible to estimate the intrinsic permeability and the slope of the Klinkenberg's law which can be used to calculate air transport under pressure from a technique of permeability measurement under vacuum, with an overestimation of about 60%.

5 In-field permeability measurement on the inner wall of an NCB mock-up

This section presents the location, the values and the analysis of the permeability in-field measurements conducted on the VeRCoRS mock-up (Figure 7). As shown in the literature, there was a lack of permeability data to precisely analyse the porosity leakage of the mock-up [17] and more generally of NCB. The aim of these measurements was to build up an experimental database to quantify the mean and the scatter of the air permeability of the concrete constituting the mock-up.

5.1 VeRCoRS mock-up description and locations of measurements

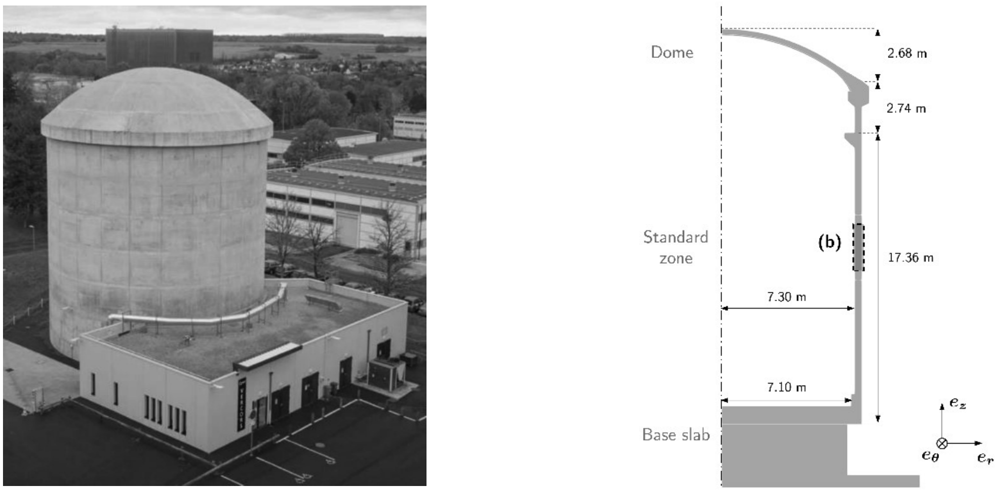

(a) (b)

Figure 10: Experimental 1:3 scaled double-walled nuclear containment building (NCB) – VeRCoRS mock-up: overview – photo by eDF (a) and 2D-AXIS view of the VeRCoRS mock-up's inner wall [46] *(b)*

A network of 80 points (Figure 11) was chosen on this 40 cm thick wall, along two horizontal lines (30 points named HL along one fifth of the circumference of the mock-up in the lower part at level 1.63 m, and 22 points named H2 along the whole circumference in the upper part at level 12.2 m) and along three vertical lines (5 points named V3 along the lower 2 meters for the angle of 80 grad, 13 points named V2 along the whole height at 190 grad and 11 points named V3 along the whole height at 330 grad). The location of the points for the permeability measurements was chosen to be representative of the concrete wall (usually far from any singularity, e.g., prestressing anchorages, gusset) and distributed on the structure (Figure 11), especially for H2, V1 and V2, to evaluate the variability of concrete on the whole structure. The distances between successive points were shortened for the lines HL (in the same batch) and V3 (different batches) to assess the dispersion of measurements in a restricted area of the structure.

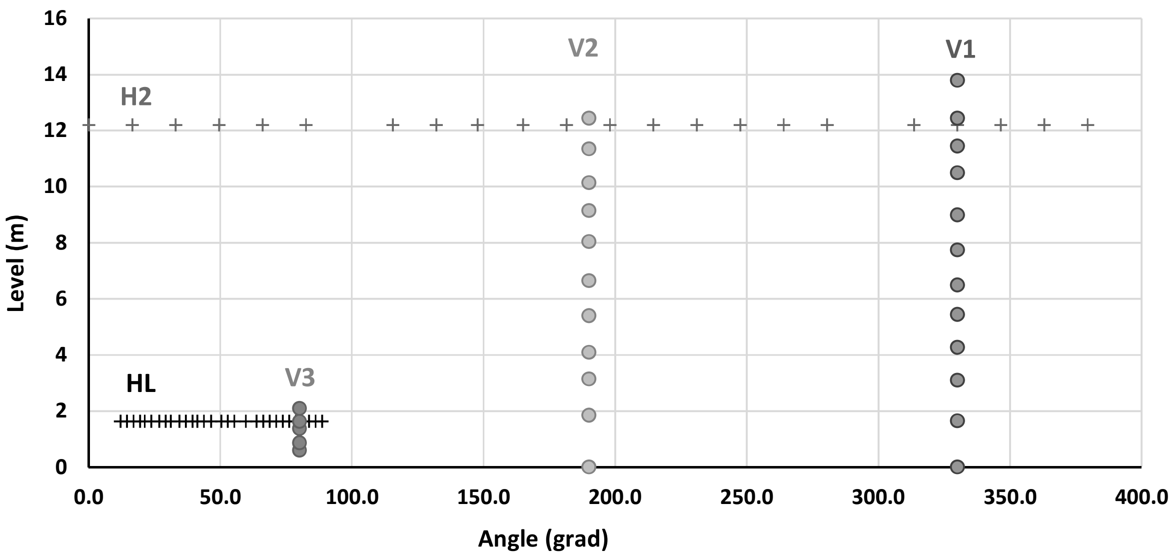

Figure 11: Locations of the 80 points for local measurements of permeability.

5.2 Measurements along horizontal and vertical lines

The distributions of both the intrinsic permeability and the slope for Klinkenberg's law obtained from the 80 measurements performed on the mock-up are presented in Figure 12. This evaluation was performed from an apparent permeability obtained in vacuum and from Eq. 10 and Eq. 11. Means and standard deviations are given in **Table 3**. Since the two parameters were evaluated from the same measurements, their distributions were similar (Figure 12). It is important to note that a measurement is very localized, with a surface of 40 mm in diameter (Torrent apparatus). Even with 80 points, the surface area investigated was very small compared to the total surface area of the mock-up. Moreover, the measurement was superficial: the air flow reached an average depth of 70 mm (Eq. 2) for a wall of 400 mm of total depth, which finally represents only 17.5% of the thickness investigated. In the field, the air permeability is not homogeneous in the thickness investigated by the technique due to the moisture gradient usual in the skin of concrete structures. Moreover, the skin of a concrete structure presents a greater proportion of mortar than the core concrete does. However, the proportion of the skin that is more permeable than the core does not impact the pressure increase during in-field measurements as the pressure increase is mainly driven by the less permeable zone of the investigated depth.

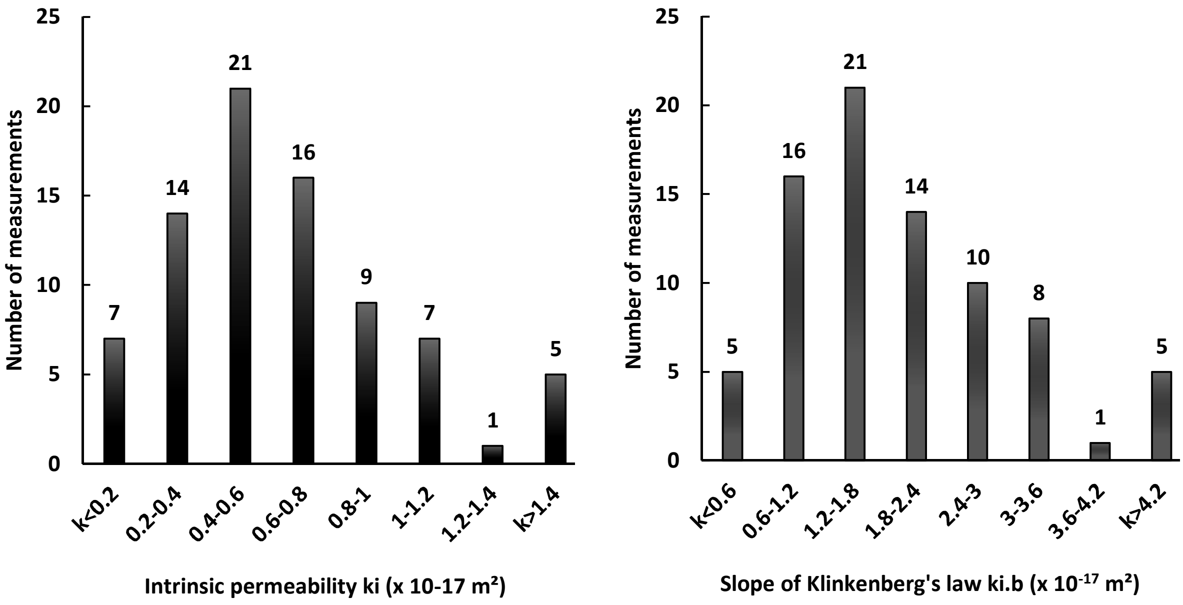

(a) (b)

Figure 12: Distributions of the intrinsic permeability (a) and of the slope of Klinkenberg's law (b) for 80 measurements performed on VeRCoRs mock-up

Table 3. Intrinsic permeability and slope of Klinkenberg's law for the whole distribution (in brackets the value when five points with very high intrinsic permeability are excluded)

	k_i (x 10^{-17} m²)	k_i . b_K (x 10^{-17} m²)
Number of measurements	80 (75)	80 (75)
Mean	0.677 (0.58)	2.075 (1.77)
Standard deviation	0.51 (0.29)	1.562 (0.89)

The mean intrinsic permeability in field is about 0.68 x 10^{-17} m² with a coefficient of variation greater than 75%. The mode is lower than the mathematical mean, the distribution is not symmetric and seems to be lognormal. The distribution was significantly influenced by the presence of five points with very large permeability (above 1.4 x 10^{-17} m²), which may correspond to points with important defects. These five measurements represent isolated values lying between 4.3 and 9.6 x 10^{-17} m², which are grouped in the last interval for the sake of simplification. Without these five points, the mean value was only about 0.58 x 10^{-17} m² with a coefficient of variation of about 50%. Such permeability can be obtained for saturation ratios between 35 and 50% (Figure 7). This value is in agreement with the water content measured in field [34].

The variations of permeability along both the horizontal and the vertical directions are presented in Figure 10 and **Table 4**. The horizontal line HL shows considerable scatter in permeability, particularly close to the angle of 80 grad (Figure 10) with 3 outliers. This area with high permeability corresponds to the 2 high values of permeability encountered for V3 (angle of 80 grad and height of about 1.6 m). The measurements along the other horizontal line (H2) present a scatter representative of the concrete heterogeneity. The permeability does not seem to be significantly dependent on the level of concrete (Figure 10-b). Except for 5 outliers, the permeability is quite homogeneous in the whole structure (**Table 4**) despite the use of several batches to cast the full height.

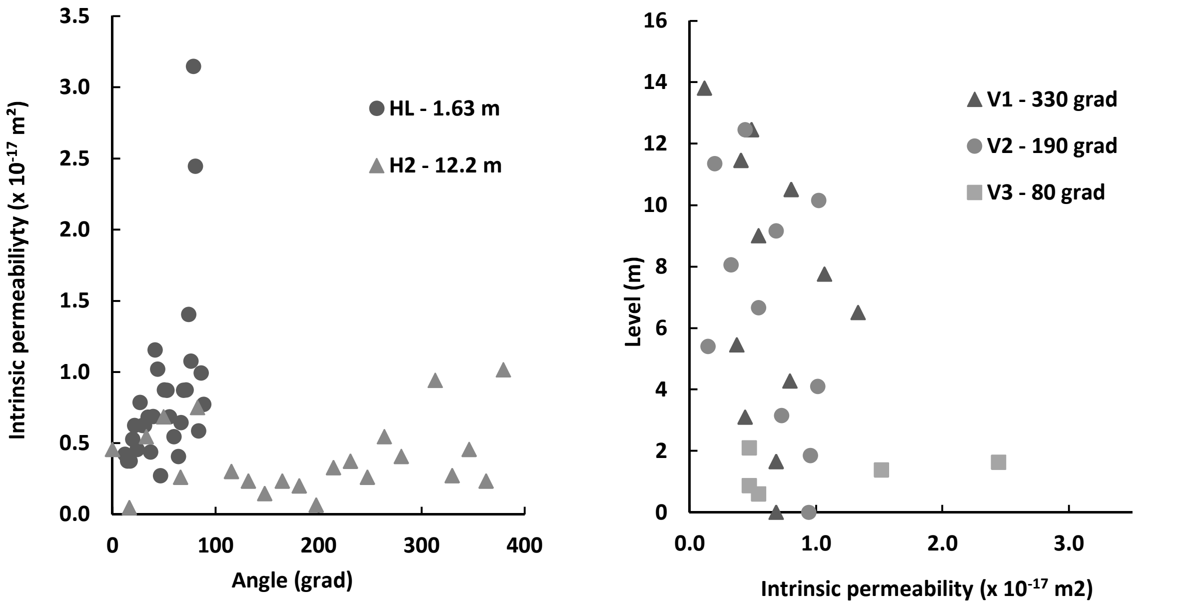

(a) (b)

Figure 13: Intrinsic permeability along two horizontal lines (a) and three vertical lines (b) of VeRCoRs mock-up

Table 4. Intrinsic permeability by measurement lines (in brackets, excluding five points with very high permeability)

Lines	HL	H2	V1	V2	V3
Number	30 (27)	22	12	11	5 (3)
Mean	0.84 (0.68)	0.40	0.64	0.64	1.09 (0.50)
Standard deviation	0.60 (0.23)	0.26	0.33	0.33	0.88 (0.08)

With the measurements performed in field, it was possible to evaluate the distribution of the intrinsic permeability along the horizontal and the vertical directions of the mock-up. It is an essential input data of the modelling presented in the following part to evaluate the porosity leakage of the mock-up, and for all future numerical modelling of the structures which can be based on the previous works presented in [14–16].

6. Air leakage calculations using Stochastic Finite Element Methods

The objective of this section is to evaluate the spatial variability of the intrinsic permeability k_{i0} of the concrete of the VeRCoRs mock-up, and its effect on the leakage rate of the structure. The spatial variability is necessary to propose a stochastic evaluation of the air leakage of the mock-up and finally to be able to estimate a potential leakage whatever the location of the considered structure. In this perspective, random fields are used for modelling the permeability, and their underlying correlation structure is identified from the non-destructive permeability measurements presented in Section 5.

The permeability measured in field on the concrete skin was only representative of the permeability in the first few centimetres of concrete, and thus, at a certain saturation degree (about 40%). To obtain the global evaluation of the leakage, the saturation evolution with depth had first to be evaluated by modelling. In the calculations presented below, the permeability along the first few centimetres was taken equal to the in-field measurement. The evolution of the permeability with depth was then calculated by the modelling from the laboratory results for the evolution of permeability with saturation as explained in part 6.2 The stochastic FE leakage model adopted in this study is subsequently presented, before probabilistic predictions of the leakage rate of the VeRCoRs mock-up are performed.

6.1 Construction of permeability random fields

Let $(\Omega, \mathscr{F}, \mathbb{P})$ be a probability space, and $\mathcal{D} \subset \mathbb{R}^3$ be the spatial domain studied. The concrete intrinsic permeability ki_0 is represented by a random field that corresponds to a family $K_{i0}(x,)_{x \epsilon D}$ of real-valued random variables defined on the underlying probability space $(\Omega, \mathscr{F}, \mathbb{P})$, which is indexed by points of the domain $\mathcal{D}$. Then, the intrinsic permeability field may be seen as a function $K_{i0}(x,\omega)_{x \epsilon D}$ of two variables, namely a spatial coordinate $\boldsymbol{x} \in D$ and a generic outcome $\omega \in \Omega$ of the underlying probability space. The permeability field K_{i0} is assumed to be a lognormal random field [46,47] and, for the sake of simplicity, the field $logK_{i0}$ is assumed to be stationary, i.e. its mean function $\mu_{logK_{i0}}$ is assumed to be constant, and its covariance kernel depends only on relative spatial coordinates, which can be written:

$$C_{logK_i}(x,x') = C_{logK_{i0}}(x - x') = \sigma^2_{logK_{i0}} R_{logK_{i0}}(x - x') \qquad \textit{Eq. 12}$$

where $\sigma^2_{logK_{i0}}$ is the variance and $R_{logK_{i0}}$the correlation kernel of the field logK_{i0}. Thus, the log-permeability random field $K_i logK_i$ is fully characterized by its moments $\left(\mu_{logK_{i0}}, \sigma^2_{logK_{i0}}\right)$, and its correlation kernel $R_{logK_{i0}}(x - x')$.

The correlation structure of the log-permeability field is identified from non-destructive permeability measurements. Only the HL measurement set (see Section 5.2) is used with sufficiently fine spacing (approx. 0.3 m between two points). Assuming that the volume concerned by measurements has a water saturation ratio of 50%, a mean of about $\mu_{K_0} = 7.10^{-17}$ m² and a CoV of 75% are estimated from measurements presented in Section 5.2. The associated experimental unidimensional (semi) variogram [48] is given by:

$$\gamma_{HL}(h) = \sigma^2_{logK_{i0}} - C_{logK_{i0}}(h v_{HL}) \qquad \textit{Eq. 13}$$

where $h > 0$ and v_{HL} is the direction of the HL line. This experimental variogram is subsequently fitted by several classical variogram models (linear, exponential and Gaussian models [48] in Figure 14). The results obtained suggest that the Gaussian model provides the best fit, with an autocorrelation length ℓ_{ac} in the direction of the HL line. For the sake of simplicity, the log-permeability random field $\log k_0(\boldsymbol{x}, \omega)$ is assumed to be isotropic, since measurements in the vertical and radial directions are not available for constructing variograms in the three main directions. Eventually, the following correlation kernel $R_{logK_i 0}(x - x')$ is considered for the log-permeability field:

$$R_{logK_{i0}}(x - x') = R_{HL}\ \left(\left\|x - x'\right\|\right) = exp\left(\frac{-1}{2}\frac{\left\|x - x'\right\|^2}{l^2_{ac}}\right) \qquad \textit{Eq. 14}$$

where $\|\cdot\|$ is the Euclidean norm of $\mathbb{R}^3$.

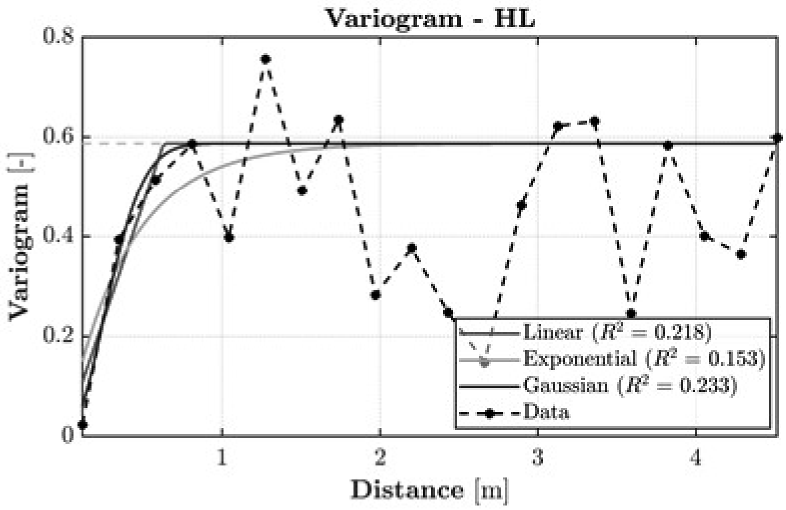

Figure 14: Experimental variogram fitting using HL measurement data.

Then, the (continuous) random field $K_{i0}(x, w)$ is approximated by a finite set of random variables $(\zeta_j)_{1\leq j\leq r}$. In this study, we focus on three main Representative Structural Volumes (RSV) [46] of the VeRCoRs mock-up; namely its standard zone (or wall), its gusset, and its dome, all depicted in Figure 15. Three finite element meshes corresponding to these RSV are considered (see Figure 15-a-c) with a characteristic mesh size of about $l_{FE} = 0.15$ m, following recommendations of [49] concerning the discretization of random fields on an FE mesh ($l_{FE} \leq l_{ac}/3$). Moreover, each mesh corresponds to an angular sector of $15°$, in order to provide dimensions larger than the fluctuation length (given by $\ell_{\text{flu}} = \sqrt{\pi}\ell_{\text{ac}} = 0.89$ m in the case of a Gaussian covariance kernel [50]) in the tangential direction. For the wall, a height of 1.5 m was chosen for the same reason, whereas full vertical dimensions were chosen for the dome and the gusset. Information concerning the geometry and the mesh of each RSV is summarized in **Table 5**.

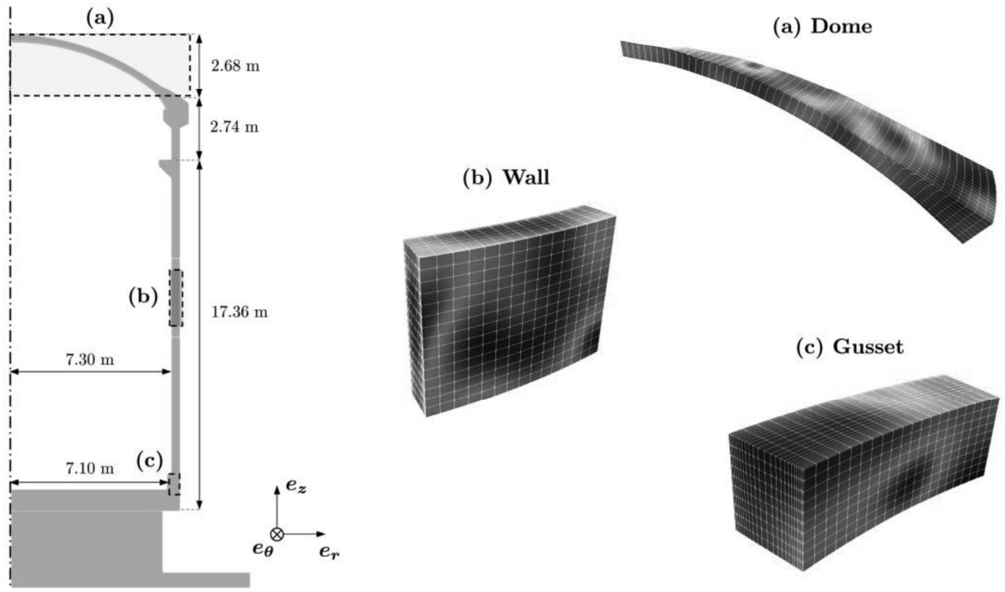

Figure 15: 2D view of the VeRCoRs mock-up (left) and some realizations of the intrinsic permeability random field on meshes of three Representative Structural Volumes (RSV) of the mock-up (right).

Table 5. Geometry and mesh of RSVs of VeRCoRs mock-up

RSV	Height [m]	Angular sector [°]	Nodes	Elements (HEXA8)
Wall	1.5		4352	3600
Gusset	0.68	15	5775	4800
Dome	2.68		7097	5910

Then, for each RSV, the log-permeability field was discretized on the corresponding FE mesh by employing the Expansion Optimal Linear Estimation (EOLE) introduced in [51]. The latter is based on a truncated version of the Karhunen-Loève (KL) expansion [49] of the log-permeability field so that the supremum norm of the error variance is below 5%. Examples of random realizations of the permeability field discretized on VeRCoRs RSVs are presented in Figure 15-a, b, and c.

6.2 Finite element leakage model

The pressurized dry air transport through a porous network is usually split into two main modes [15,17]:

- diffuse porosity leakage (Darcy's mode), which refer to the leakage through concrete porosity or through micro cracks
- localised leaks, mainly driven by the leakage through concrete macro cracks, associated with Poiseuille's flow mode

This paper focuses on the Darcy's transport mode and describes a chained calculation involving the computation of the thermal, hydric and hydraulic responses. Only gas transport through sound porous concrete is considered, and the gaseous phase is assumed not to contain any vapour. The dry air leakage is modelled by the following macroscopic diffusive equation:

$$\frac{d}{dt}P(x,t) = \frac{d}{dx}\left(\frac{k_a(x,t)}{2\mu}\frac{d}{dx}P^2(x,t)\right) \quad \textit{Eq. 15}$$

where P is the dry air pressure, μ the air dynamic viscosity, and k_a the Darcy's apparent permeability of concrete (evaluated according to saturation ratio and pressure at the location under consideration in the wall).

The Darcy's apparent permeability term k_a is described with the following model

$$k_a(x,t) = k_i(x)\alpha_k(x,t) \quad \textit{Eq. 16}$$

where k_i is the intrinsic permeability of concrete depending on the saturation ratio:

$$k_i(x) = k_{i0}(x)k_{rg}(x,t) \quad \textit{Eq. 17}$$

with k_{i0} the intrinsic permeability of concrete in the dry state, k_{rg} the relative gas permeability of concrete, and α_K a multiplicative factor accounting for the Klinkenberg effect, given by:

$$\alpha_K(x,t) = 1 + \frac{b(x,t)}{P_m} \quad \textit{Eq. 18}$$

where $b_K(x,t)$ is the Klinkenberg coefficient, and P_m, the mean difference between the atmospheric pressure and the pressure of the test.

Both relative gas permeability k_{rg} and the Klinkenberg coefficient b_K are assumed to be dependent on the water saturation ratio of concrete, denoted by S_w. These functions are defined only by the mean experimental curves given in Figure 7. No special variability is considered for these input data as it has been verified that, compared to the spatial variability of permeability obtained in field, the input data variability has a negligible impact on the final prediction.

The water saturation ratio, $S_{w,}$ is calculated through the chained thermo-hydric modelling strategy presented in [52]. Concerning thermal calculations, linear Neumann boundary conditions are considered on internal and external surfaces, by using in-situ measurements of the temperature of the ambient air of the structure. For hydric calculations, linear relative humidity (RH) fluxes are imposed on both internal and external surfaces, by using measured histories of the ambient air RH. The measured histories of ambient temperature and RH are given in Figure 16. During the first year after the start of construction of the mock-up, the RH and the temperature of the ambient air followed seasonal conditions. Then, in order to simulate an operating reactor, a heating system was started around 1.5 years after the beginning of construction, in order to increase the temperature of the inner ambient air to about 35°C. The temperature of the ambient air outside the mock-up inner wall was controlled, to be stabilized around 20°C (see Figure 16-b). Due to the increase of the inner air temperature, the RH of the inner air decreased to about 20% (see Figure 16-a) while the RH of the ambient air outside the mock-up inner wall fluctuated around a value of 50%. A few weeks before each pressurization test of the mock-up, the temperature of the inner air was decreased to about 15°C. This temperature was maintained for a few weeks after the end of the pressurization test (see Figure 16-b). Due to the correlation existing between temperature and RH (typically expressed by

Magnus' law), this temperature decrease induced an increase of the ambient air RH, up to a value of about 80%.

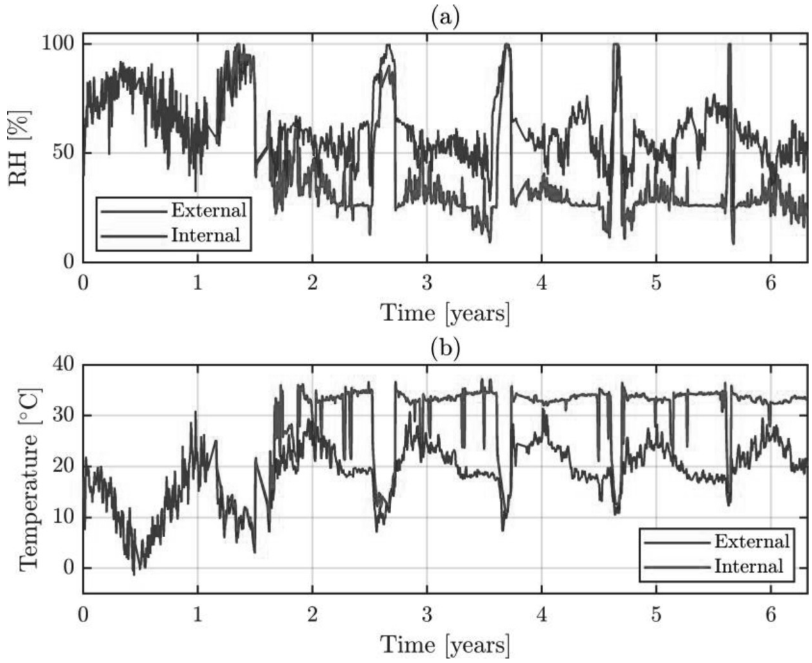

Figure 16: Measured ambient conditions of the VeRCoRs mock-up : (a) RH ; (b) temperature .

Saturation profiles that were computed through a single deterministic calculation with the same thermo-hydric model and boundary conditions (BC) are presented in Figure 17. Firstly, the water saturation in the concrete volume decreases slightly over the 1st year. Then, due to the activation of the heating system, the water saturation decreases faster, reaching a mean value of about 80% at t=2 years. Then, water saturation decreases to a mean value of about 65% at t =6 years (about 75% in the core of the wall and lower saturation ratio close to the external surfaces). In the following, the parameter B of the drying model and the initial water content $C_{w,0}$ of concrete are considered as random parameters.

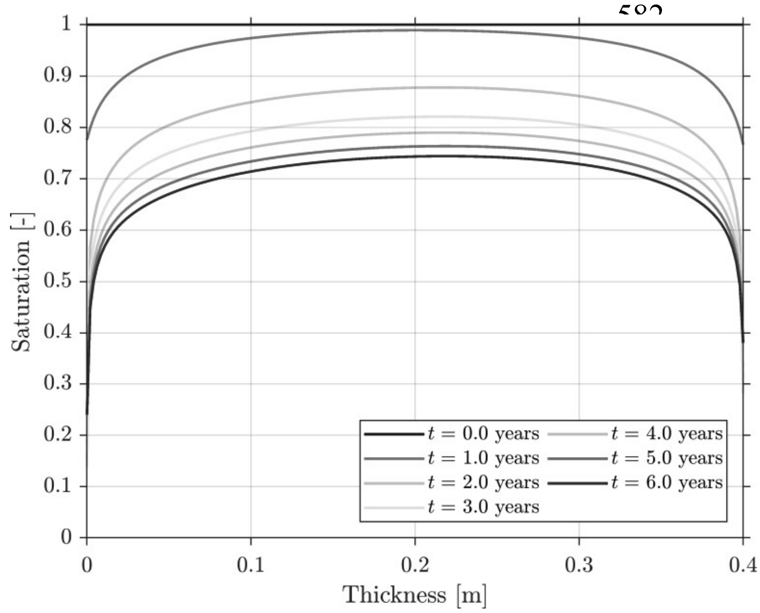

Figure 17: Water saturation profiles in the thickness of VeRCoRs' standard zone, computed through a single deterministic calculation with the adopted thermo-hydric FE model. Intrados is located at 0 m in the wall thickness.

Finally, the pressure boundaries considered were of the Dirichlet Type (overpressure on the intrados side) and the evolution was descriptive of the periodic pressurization tests. During each test, the internal air pressure was gradually increased until it reached an absolute pressure of 5.2 bars. Pressure histories associated with each test may be found in [47]. The structural Darcy's leakage rate was computed from the pressure field obtained by solving Eq. 15 and by integrating Darcy's flux on the external surface of the structure:

$$q(x,t) = \frac{-k_a(x,t)}{\eta_a}\frac{d}{dx}p(x,t)$$

$$Q(t) = \int_{S_x \epsilon S_{ext}} q(x,t)dS_x \qquad \textit{Eq. 19}$$

6.3 Probabilistic diffuse leakage calculations

6.3.1. Uncertainty propagation with Polynomial Chaos Expansions (PCE)

For a given RSV, the diffuse leakage rate, Q, computed with the leakage model described in Section 6.1 may be seen as a function of d input random variables $X: \Omega \rightarrow D_X \subset R^d$, which represent the uncertain parameters of the leakage model. In this contribution, three parameters are modelled by random variables in addition to the intrinsic permeability k_{i0}, which is represented by a discretized random field (see Section 6.2). These three additional parameters are given by:

- the parameter B of the drying model adopted (see [25, 29, 35]), which drives the drying speed of the concrete volume,
- the initial water content $C_{w,0}$ of concrete,
- Klinkenberg's slope $k_i \cdot b_K$.

This choice is justified by the fact that earlier studies have identified these parameters as those having the most influence on the diffuse leakage response at structural scale (see, e.g., [46]). The characteristics of the random parameters $(B, C_{w,0}, b_K)$ and field k_0 are summarized in **Table 6**. The parameters $(B, C_{w,0}, b_K)$ are assumed to be uniform in the structure for each calculation, while the permeability, k_0, is spatially variable, since it is modelled by a random field. We recall that the Karhunen-Loève eigenmodes of the intrinsic permeability random field are uncorrelated standard normal random variables. Furthermore, all the input parameters considered are assumed to be mutually independent.

Table 6. Characteristics of the input random parameters and the intrinsic permeability field.

Parameter	Notation	Unit	Distribution	Mean	Standard deviation	CoV
Drying parameter	B	-	Lognormal	0.08	0.016	0.2
Initial water content	$C_{w,0}$	$l.m^{-3}$	Lognormal	145	29	0.2
Klinkenberg's coefficient	b_K	MPa	Lognormal	0.18	0.09	0.5
Intrinsic permeability in dry state	k_0	10^{-17} m^2	Lognormal	7.0	5.25	0.75

Then, the quantification of the uncertainties on the leakage rate Q induced by the uncertainties on the inputs is typically achieved through a Monte Carlo approach, by drawing a large sample ($\sim 10^5 \quad 10^6$) of X and subsequently computing the corresponding output leakage rates with the FE model.

For cost efficiency (compared to the Monte Carlo approach), surrogate modelling allows the construction of a cheap approximation of the input-output map provided by the FE model, in order to notably reduce the computational burden of uncertainty propagation. In this context, Polynomial Chaos Expansions (PCE) [54] are widely used. The leakage response $Q(X)$ provided by the FE model is then approximated by a PCE, which consists of a truncated series expansion formed by orthonormal polynomials [54]. Further details about the PCE surrogates constructed are given in Appendix A. Then, the constructed PCE surrogate models enable a global sensitivity analysis of the leakage response to be performed with respect to the input random variables of the model. Sobol's sensitivity indices [55] may be computed as a by-product of PCE, through analytical formulas involving PCE coefficients [56]. The time evolution of the total Sobol indices of the diffuse leakage response of the structure's wall is presented in Figure 18.

Firstly, the drying parameter B contributes most to the variance of the diffuse leakage response, since its total order Sobol index is significantly larger than the Sobol indices of the other parameters (Figure 18). It is also worth noting that only the first KL eigenmode ζ_1 of the intrinsic permeability random field contributes significantly to the output variance. This might be explained by the fact that the diffuse leakage rate is computed by integrating a Darcy flux on the external surface of the structure, which induces a homogenization of fluctuations of the permeability random field. For this reason, the diffuse leakage response is only sensitive to large scale fluctuations of the permeability field. Moreover, the sum of all Sobol indices is significantly larger than 1, notably before t=3 years, which indicates the presence of interactions between parameters.

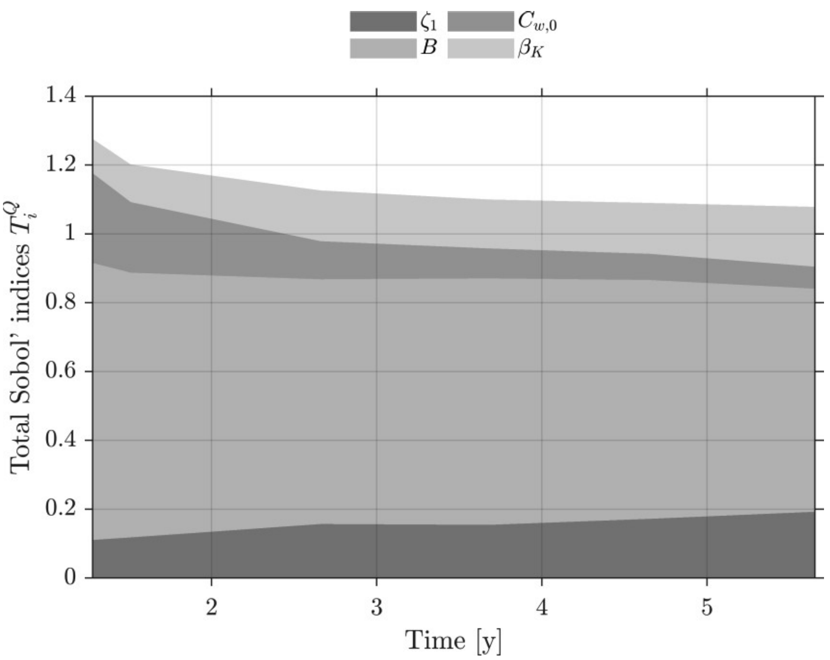

Figure 18: Time evolution of total of Sobol sensitivity indices of the diffuse leakage rate

In order to further investigate such interactions, the most significant second order Sobol indices of the diffuse leakage response are presented in Figure 19. The drying parameter, B, presents significant interactions with the intrinsic permeability RF eigenmode ζ_1, the initial water content $C_{w,0}$ and the Klinkenberg coefficient b_K. The contribution of these interactions decreases over time, which emphasizes the long-term behaviour of the sum of total Sobol indices, expressing a decrease in the importance of interactions.

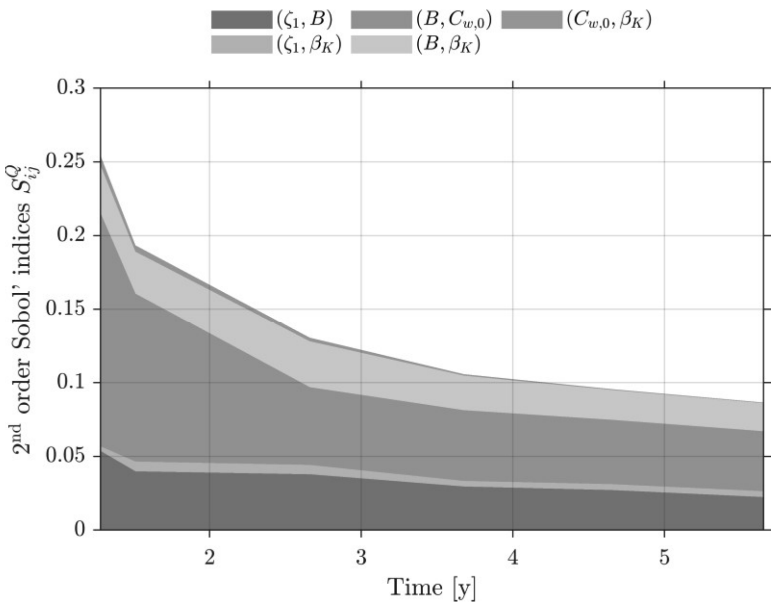

Figure 19: Time evolution of second order Sobol sensitivity indices of the diffuse leakage rate.

Finally, the global sensitivity analysis conducted underlined the very strong importance of drying parameters for the variability of the diffuse leakage response. Thus, in spite of the significant contribution of the permeability field to the variance of the leakage response, the variability of drying parameters must not be ignored when quantifying the uncertainties of the diffuse leakage response.

6.3.2. Probabilistic diffuse leakage calculations

The uncertainties of the input random parameters are propagated through the PCE surrogate model in order to compute the time evolution of the diffuse leakage rate of the VeRCoRs mock-up, together with related statistical quantities of interest such as mean and standard deviation. Before presenting a comparison of the time evolution of the predicted and measured VeRCoRs diffuse porosity leakage rates, the global leakage measurements conducted on the VeRCoRs mock-up are discussed, and presented in Figure 20. Diffuse leakage measurements are obtained in an indirect way: the global VeRCoRs leakage rate is assumed to be a superposition of two main contributions, namely Darcy leakage through concrete porosity (i.e. diffuse leaks) and leakage through cracks and possibly other types of defects (e.g. steel/concrete interfaces, casting joints) [10]. The global leakage rate is directly measured with acceptable confidence, whereas the contribution of cracks is (partially) measured with leakage collecting boxes, after a visual inspection intended to locate such defects [10,57]. This measurement process presents significant uncertainties (accuracy of the measuring device according to measured air flow, quantification of the length of defects, etc.) which are transferred to the estimation of the diffuse leakage of the structure, knowing that it is computed by subtracting the total leakage of cracks from the global leakage rate. This is underlined by the fairly large error bars of the observed diffuse leakage rate shown in Figure 20. These error bars represent the 68% confidence level (i.e. the mean plus or minus one standard deviation, assuming a Gaussian distribution for measurements).

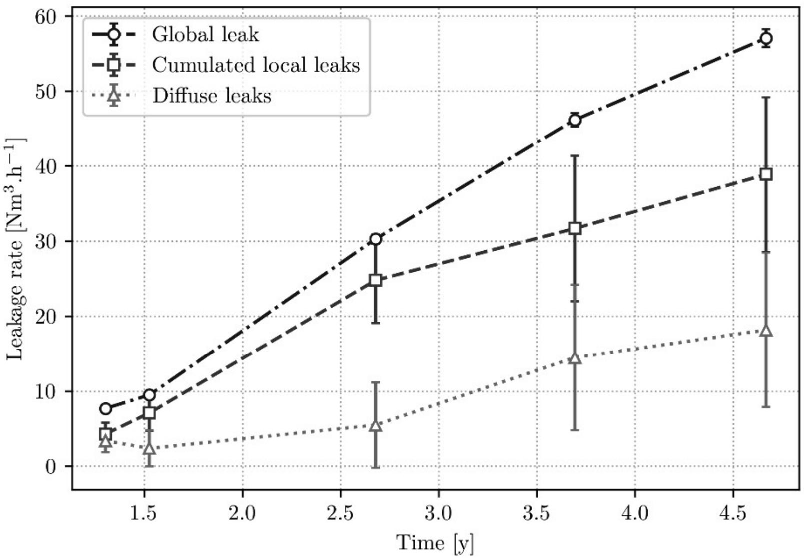

Figure 20: Measurements of the global, local and diffuse leaks of VeRCoRs mock-up during pressurization tests. Error bars correspond to 68 % CI (i.e. mean ±standard deviation), assuming Gaussian distributions for measurements

A comparison of the probabilistic predictions of the diffuse leakage rate and its measured counterpart is presented in Figure 21.

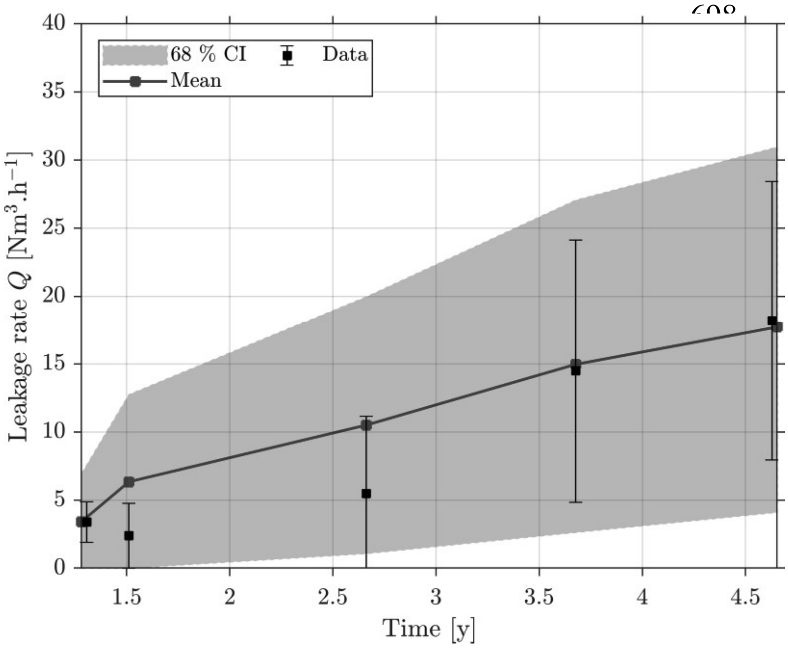

Figure 21: Probabilistic diffuse leakage predictions and comparison with measurements

Diffuse leakage predictions are in very good agreement with measurements, especially concerning the first and the last two pressurization tests of the VeRCoRs mock-up. At the fifth VeRCoRs pressurization test (∼ 4.8 years), the mean predicted leakage rate (17.7 $Nm^3.h^{-1}$) approaches the mean observed diffuse leakage rate (18.2 $Nm^3.h^{-1}$) with a relative error of about 3%. The modelling of the spatial variability of permeability based on surface in situ measurements in vacuum (investigated depth about 70 mm) and drying parameters based on previous analysis [46,53] led to a reliable predictive evaluation of the diffuse leakage rate for 400 mm thick concrete wall. The assumption of a mean saturation degree on the investigated depth during measurements in the field is sufficient to obtain a realistic evaluation. Most of the previous numerical studies performed with the leakage results obtained on the VeRCoRs mock-up focused on the determination of the leakage through cracks [14,15]. Compared to the study with a specific focus on the porosity leakage rate for the VeRCoRs mock-up [17], the use of in field measurement proposed in the present work helps to obtain a more accurate prediction. This work should help to accurately separate leakage from crack leakage when evaluating the tightness of structures.

In this work, the evolution of the permeability with saturation degree was evaluated on laboratory concrete samples after 60 days in limewater. Since the cement used was a CEM I, the hydration should be quite stabilized after this period [20], but in real structures the hydration could still have progressed after several years of atmospheric exposure. In the zones exposed to dry conditions (concrete skin), the saturation level should be too low to induce additional hydration for the cement. In the centre of the wall, the higher saturation conditions can lead to additional hydration and thus to have lower permeability in the structure than in laboratory. But the permeability used in the calculations was directly measured in field and only the dependences to saturation degree and pressure can have been impacted by the differences between laboratory and field. This could have led to a small misestimation of the leakage by the model. An overestimation was observed for the early age of the structure (before 3.5 years) and decreased with time. Combinations with other phenomena, such as the progressive drying of concrete / steel interfaces, could have a greater impact than the modification of permeability by cement hydration.

A stochastic element finite approach was used to characterize the leakage rate of the VeRCoRs mock-up. The range given by the 68% credible bounds of the predicted diffuse leakage rate is quite close to the experimental one. Predictions overestimate the measured leakage rates during the second and third tests but values measured during these tests are nevertheless included in the confidence bounds of predictions. It is also worth noting that the global measurements present a sudden evolution between the third and the fourth pressurization tests. This might be attributable to the quite large uncertainties on measurements, which tend to increase over time (due to the fact that the number of local leaks increases and that larger local leaks are measured with less accurate flowmeters), and also to several physical processes related to drying.

7. Conclusion

In this contribution, the air leakage through concrete is estimated using a novel testing technique coupled to stochastic finite element (SFE) modelling.

The main results of the studies are:

- For the first time, both the intrinsic permeability and the slope of Klinkenberg's law were evaluated from in-field measurements under vacuum using a methodology previously proposed from a laboratory study in [12],
- 80 vacuum measurements collected on the VeRCoRs mock-up allowed the spatial variability of intrinsic permeability to be characterized,
- The permeability data collected in the field were used to evaluate the diffuse leakage of a real structure. In the case of the VeRCoRs mock-up, an SFE model of the air leakage was built: it leads to an estimation of the mean response that is globally accurate (difference of less than 10% on the flow obtained on the structure) in terms of the diffuse air leakage under pressure),
- SFE modelling allows also the quantification of the uncertainties around the predicted values over time.

In situ measurements show discrepancies in concrete permeability properties. Such variations are associated with the intrinsic variation of the porosity of concrete coupled with drying and microcracking phenomena. For the probabilistic diffuse leakage calculations, the parameters of both drying and permeability equations were considered as random parameters:

- The contribution of the permeability field to the variance of the leakage response was significant (always greater than 25%).

- The variability of the drying parameters (even if they are assumed to be homogeneous in structure) cannot be ignored in order to obtain a reliable quantification of the diffuse leakage uncertainties.

Acknowledgements

The authors acknowledge the financial support provided by MACENA and ENDE project funds (ProjetIA-11-RSNR-0009 and ProjetIA-11-RSNR-0012). The opinions presented in this paper reflect those of the authors only and do not necessarily represent the opinions of the funding agencies.

Appendix A: Polynomial Chaos Expansions

The input-output map given by the diffuse leakage rate Q described in Section 6.3 is approximated by a Polynomial Chaos Expansions (PCE) surrogate model, which consists of a truncated series expansion formed by orthonormal polynomials [54]:

$$Q(X) \approx \hat{Q}(X) = \sum_{\alpha\in A} a_\alpha \, \Psi_\alpha(X) \qquad \text{Eq. 20}$$

where $A \subset N^d$ is a set of multi-indices, $(a_\alpha)_{\alpha\in A}$ the PCE coefficients, and for $\alpha = (\alpha_{1,\dots,}\alpha_d) \in A \Psi_\alpha$ is the tensorized multivariate Hermite polynomial defined by:

$$\Psi_\alpha(X) = \prod_{i=1}^{d} \psi_{\alpha_i}^{(i)}(X_i) \qquad \text{Eq. 21}$$

where $\psi_{\alpha_i}^{(i)}$ is the univariate Hermite polynomial of degree $\alpha_i \in N$.

In this work, the PCE coefficients $(a_\alpha)_{\alpha\in A}$ are computed with the procedure introduced in [58], based on the Least Angle Regression algorithm (LARS). The goodness of fit between the PCE and the FE model response is quantified by computing the so-called Leave One Out (LOO) validation error (see [58,59] for further details).

For each pressurization test and each RSV described in Section 6.1, a PCE of the diffuse leakage response is constructed, by considering an experimental design of size $N = 500$, generated with the Latin Hypercube Sampling (LHS) method [60]. It is worth noting that the leakage rate of the gusset RSV may be treated as negligible, since its maximal value is smaller than 0.1 $Nm^3.h^{-1}$. This may be explained by the greater thickness of the gusset (0.6 m), which induces a larger water saturation ratio in the thickness, a smaller pressure gradient, and consequently a lower diffuse leakage rate. Conversely, the standard zone of the structure is the main contributor to the total diffuse leakage rate (approx. 90%), especially due to its large surface area.

A comparison between the structural diffuse leakage rate responses computed with the FE model and the corresponding PCE-based responses is given in Figure 20. The PCE surrogate provides a satisfactory approximation of the FE model leakage response, as underlined by the good agreement observed between point-wise evaluations. Furthermore, the maximal LOO validation error is about 0.03, which is an acceptable error level, compared to the threshold values of about 0.05 usually considered in engineering practice [46,53].

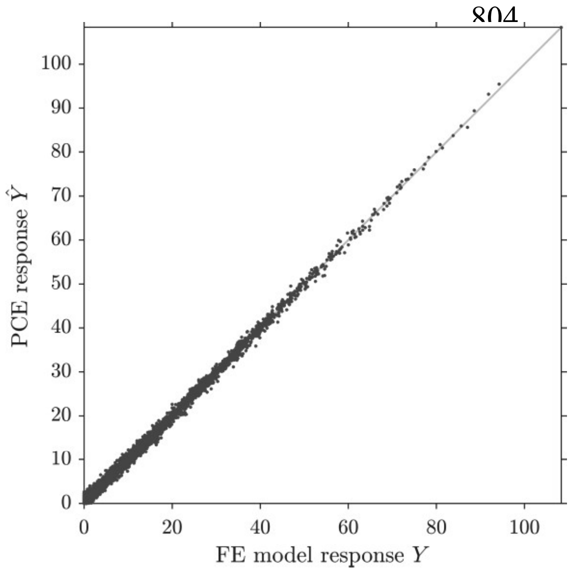

Figure 22: Cross-plot of the PCE surrogate of the structural diffuse leakage rate response.

References

[1] J.J. Kollek, The determination of the permeability of concrete to oxygen by the Cembureau method-a recommendation, Mater. Struct. 22 (1989) 225–230. https://doi.org/10.1007/BF02472192.

[2] R.J. Torrent, A two-chamber vacuum cell for measuring the coefficient of permeability to air of the concrete cover on site, Mater. Struct. 25 (1992) 358–365.

[3] P. Basheer, F. Montgomery, A. Long, “CLAM” tests for measuring in situ permeation properties of concrete, Nondestruct. Test. Eval. 12 (1995) 53–73.

[4] Z. Lafhaj, G. Richard, M. Kaczmarek, F. Skoczylas, Experimental determination of intrinsic permeability of limestone and concrete: Comparison between in situ and laboratory results, Build. Environ. 42 (2007) 3042–3050. https://doi.org/10.1016/j.buildenv.2006.07.039.

[5] J. Liu, F. Agostini, F. Skoczylas, From relative gas permeability to in situ saturation measurements, Constr. Build. Mater. 40 (2013) 882–890. https://doi.org/10.1016/j.conbuildmat.2012.11.092.

[6] K. Yang, P.A.M. Basheer, Y. Bai, B.J. Magee, A.E. Long, Development of a new in situ test method to measure the air permeability of high performance concretes, NDT E Int. 64 (2014) 30–40. https://doi.org/10.1016/j.ndteint.2014.02.005.

[7] D. Zhang, K. Li, Concrete gas permeability from different methods: Correlation analysis, Cem. Concr. Compos. 104 (2019) 103379. https://doi.org/10.1016/j.cemconcomp.2019.103379.

[8] R.J. Torrent, R.D. Neves, K.-I. Imamoto, Concrete permeability and durability performance from theory to field applications, CRC Press, Taylor & Francis, 2022.

[9] E. Oukhemanou, S. Desforges, E. Buchoud, S. Michel-Ponnelle, A. Courtois, VeRCoRs Mock-Up: Comprehensive Monitoring System for Reduced Scale Containment Model, in: Technol. Innov. Nucl. Civ. Eng. TINCE, Paris (France), 2016.

[10] J.-M. Henault, P. Laviron, S. Desforges, D. Vautrin, A. Courtois, B. Martin, A. Legrix, How to characterize the airtightness of containment structures . Overview of monitoring techniques tested on VeRCoRs Mock up, in: Technol. Innov. Nucl. Civ. Eng., Paris (France), 2018.

[11] R. Torrent, E. Denarié, F. Jacobs, A. Leemann, T. Teruzzi, Specification and site control of the permeability of the cover concrete: The Swiss approach, Mater. Corros. 63 (2012) 1127–1133. https://doi.org/10.1002/maco.201206710.

[12] H. Sogbossi, J. Verdier, S. Multon, New approach for the measurement of gas permeability and porosity accessible to gas in vacuum and under pressure, Cem. Concr. Compos. 103 (2019) 59–70. https://doi.org/10.1016/j.cemconcomp.2019.04.032.

[13] H. Sogbossi, Etude de l’évolution de la perméabilité du béton en fonction de son endommagement : transposition des résultats de laboratoire à la prédiction des débits de fuite sur site, PhD thesis, Université de Toulouse, 2017.

[14] T. Thénint, V. Le Corvec, S. Ghavamian, Study of the containment history of the VeRCoRS mock-up and prediction of the leakage rate under pressurization tests, in: P.G. and C.L.B. (Eds) G. Pijaudier-Cabot (Ed.), 10th Int. Conf. Fract. Mech. Concr. Concr. Struct. Fram., 2019. https://doi.org/10.21012/fc10.235607.

[15] L. Charpin, J. Niepceron, M. Corbin, B. Masson, J.P. Mathieu, J. Haelewyn, F. Hamon, M. Åhs, S. Aparicio, M. Asali, B. Capra, M. Azenha, D.E.M. Bouhjiti, K. Calonius, M. Chu, N. Herrman, X. Huang, S. Jiménez, J. Mazars, M. Mosayan, G. Nahas, J. Stepan, T. Thenint, J.M. Torrenti, Ageing and air leakage assessment of a nuclear reactor containment mock-up: VERCORS 2nd benchmark, Nucl. Eng. Des. 377 (2021). https://doi.org/10.1016/j.nucengdes.2021.111136.

[16] L. Charpin, J. Haelewyn, A.C. El Idrissi, J. Niepceron, B. Masson, C. Toulemonde, G. Boulant, J.P. Mathieu, F. Hamon, S. Michel-Ponnell, J.M. Hénault, F. Taillade, J.L. Adia, F. Escoffier, Predicting Leakage of the Vercors Mock-Up and Concrete Containment Buildings - a Digital Twin Approach, Acta Polytech. CTU Proc. 33 (2022) 78–84. https://doi.org/10.14311/APP.2022.33.0078.

[17] T. Meng, L. Jason, T. Heitz, B. Richard, Numerical methodology on prestressed reinforced concrete containment building: Creep, aging and leakage. Application to VERCORS mock-up, Eng. Struct. 280 (2023) 115625. https://doi.org/10.1016/j.engstruct.2023.115625.

[18] L. Jason, Relation endommagement perméabilité pour les bétons : application aux calculs de structures, Nantes, 2004.

[19] V. Garnier, J.-M. Henault, H. Hafid, J. Verdier, J.F. Chaix, E. Al, Containment nuclear plant structures evaluation by non destructive testing: strategy and results, in: TINCE 2016, 3rd Conf. Technol. Innov. Nucl. Civ. Eng., Paris, France, 2016.

[20] V. Waller, Relations entre composition des bétons, exothermie en cours de prise et résistance en compression, PhD Thesis, École Nationale des Ponts et Chaussées, 1999.

[21] W. Ladaoui, T. Vidal, A. Sellier, X. Bourbon, Effect of a temperature change from 20 to 50 C on the basic creep of HPC and HPFRC, Mater. Corros. 44 (2011) 1629–1639. https://doi.org/10.1617/s11527-011-9723-z.

[22] W. Ladaoui, T. Vidal, A. Sellier, X. Bourbon, Analysis of interactions between damage and basic creep of HPC and HPFRC heated between 20 and 80 °c, Mater. Struct. 46 (2013) 13–23. https://doi.org/10.1617/s11527-012-9879-1.

[23] M. Ibro, J. Verdier, S. Geoffroy, H. Cagnon, X. Bourbon, Prediction of moisture transfer in cement-based materials : Use of a porous network model to access transfer parameters, Cem. Concr. Res. 142 (2021) 106310. https://doi.org/10.1016/j.cemconres.2020.106310.

[24] A. Pichelin, M. Carcassès, F. Cassagnabère, S. Multon, G. Nahas, Sustainability, transfer and containment properties of concrete subject to delayed ettringite formation (DEF), Cem. Concr. Compos. 113 (2020) 103738. https://doi.org/10.1016/j.cemconcomp.2020.103738.

[25] C. Antón, M.A. Climent, G. de Vera, I. Sánchez, C. Andrade, An improved procedure for obtaining and maintaining well characterized partial water saturation states on concrete samples to be used for mass transport tests, Mater. Struct. 46 (2012) 1389–1400.

[26] RILEM TC 116-PCD, Permeability of concrete as a criterion of its durability, final report, Mater. Struct. 32 (1999) 163–173.

[27] M. Carcassès, A. Abbas, J.-P. Ollivier, J. Verdier, An optimised preconditioning procedure for gas permeability measurement, Mater. Struct. 35 (2001) 22–27.

[28] M.P. Yssorche, J.P. Bigas, J.P. Ollivier, Mesure de la perméabilité à l'air des bétons au moyen d'un perméamètre à charge variable, Mater. Struct. 28 (1995) 401–405. https://doi.org/10.1007/BF02473075.

[29] L.J. Klinkenberg, The Permeability Of Porous Media To Liquids And Gases, in: Drill. Prod. Pract., American Petroleum Institute, 1941: pp. 200–213.

[30] V. Čalogović, Gas permeability measurement of porous materials (concrete) by time-variable pressure difference method, Cem. Concr. Res. 25 (1995) 1054–1062.

[31] X. Dérobert, J. Iaquinta, G. Klysz, J.P. Balayssac, Use of capacitive and GPR techniques for the non-destructive evaluation of cover concrete, NDT E Int. 41 (2008) 44–52. https://doi.org/10.1016/j.ndteint.2007.06.004.

[32] G. Villain, A. Ihamouten, X. Dérobert, Determination of concrete water content by coupling electromagnetic methods: Coaxial/cylindrical transition line with capacitive probes, NDT E Int. 88 (2017) 59–70. https://doi.org/10.1016/j.ndteint.2017.02.004.

[33] S. Bonnet, J.P. Balayssac, Combination of the Wenner resistivimeter and Torrent permeameter methods for assessing carbonation depth and saturation level of concrete, Constr. Build. Mater. 188 (2018) 1149–1165. https://doi.org/10.1016/j.conbuildmat.2018.07.151.

[34] S. Multon, J. Verdier, G. Villain, H. Sogbossi, X. Derobert, H. Cagnon, J.-P. Balayssac, Non-destructive measurements for the evaluation of the air permeability of concrete structures, Measurement. 196 (2022) 111204. https://doi.org/10.1016/j.measurement.2022.111204.

[35] A. Abbas, M. Carcasses, J.-P. Ollivier, Gas permeability of concrete in relation to its degree of saturation, Mater. Struct. 32 (1999) 3–8.

[36] H. Sogbossi, J. Verdier, S. Multon, Permeability and damage of partially saturated concrete exposed to elevated temperature, Cem. Concr. Compos. 109 (2020) 103563. https://doi.org/10.1016/j.cemconcomp.2020.103563.

[37] J.F. O'Hanlon, A user's guide to vacuum technology, 3ième édit, John Wiley & Sons, 2005.

[38] J.G. Heid, J.J. McMahon, R.F. Nielsen, S.T. Yuster, Study of the Permeability of Rocks to Homogeneous Fluids, in: American Petroleum Institute, 1950.

[39] R. Aguilera, Incorporating capillary pressure, pore throat aperture radii, height above free-water table, and

Winland r35 values on Pickett plots, Am. Assoc. Pet. Geol. Bull. 86 (2002) 605–624. https://doi.org/10.1306/61EEDB5C-173E-11D7-8645000102C1865D.

[40] F.A. Florence, J. Rushing, K.E. Newsham, T.A. Blasingame, Improved Permeability Prediction Relations for Low Permeability Sands, in: Society of Petroleum Engineers, 2007.

[41] T.J. Katsube, Review of formation resistivity factor equations related to new pore-structure concepts, Geological Survey of Canada, 2010.

[42] C. Perez-Rosales, On the Relationship Between Formation Resistivity Factor and Porosity, Soc. Pet. Eng. J. 22 (1982) 531–536. https://doi.org/10.2118/10546-PA.

[43] F. Khaddour, D. Grégoire, G. Pijaudier-Cabot, Capillary bundle model for the computation of the apparent permeability from pore size distributions, Eur. J. Environ. Civ. Eng. 19 (2015) 168–183. https://doi.org/10.1080/19648189.2014.939307.

[44] Y. Sakai, T. Kishi, Numerical simulation of air permeability in covercrete assuming molecular flow in circular tubes, Constr. Build. Mater. 125 (2016) 784–789. https://doi.org/10.1016/j.conbuildmat.2016.08.105.

[45] Y. Sakai, Correlations between air permeability coefficients and pore structure indicators of cementitious materials, Constr. Build. Mater. 209 (2019) 541–547. https://doi.org/10.1016/j.conbuildmat.2019.03.068.

[46] D.E.M. Bouhjiti, J. Baroth, F. Dufour, S. Michel-Ponnelle, B. Masson, Stochastic finite elements analysis of large concrete structures' serviceability under thermo-hydro-mechanical loads – Case of nuclear containment buildings, Nucl. Eng. Des. 370 (2020) 110800. https://doi.org/10.1016/j.nucengdes.2020.110800.

[47] D. Rossat, D.E.M. Bouhjiti, J. Baroth, M. Briffaut, F. Dufour, A. Monteil, B. Masson, S. Michel-Ponnelle, A Bayesian strategy for forecasting the leakage rate of concrete containment buildings – Application to nuclear containment buildings, Nucl. Eng. Des. 378 (2021) 111184. https://doi.org/10.1016/j.nucengdes.2021.111184.

[48] N. Cressie, Statistics for Spatial Data, John Wiley & Sons, Inc., 1993.

[49] B. Sudret, A. Der Kiureghian, Stochastic Finite Element Methods and Reliability - A State-of-the-Art Report, 2000.

[50] E. Vanmarcke, Random fields, analysis and synthesis, MIT Press, Cambridge, Mass, 1983.

[51] C. Li, A. Kiureghian, Optimal Discretization of Random Fields, J. Eng. Mech. 119 (1993) 1136–1154.

[52] D.E.M. Bouhjiti, M. Boucher, M. Briffaut, F. Dufour, J. Baroth, B. Masson, Accounting for realistic Thermo-Hydro-Mechanical boundary conditions whilst modeling the ageing of concrete in nuclear containment buildings: Model validation and sensitivity analysis, Eng. Struct. 166 (2018) 314–338. https://doi.org/10.1016/j.engstruct.2018.03.015.

[53] D. Rossat, J. Baroth, M. Briffaut, F. Dufour, B. Masson, A. Monteil, S. Michel-Ponnelle, Bayesian

updating for nuclear containment buildings using both mechanical and hydraulic monitoring data, Eng. Struct. 262 (2022) 114294. https://doi.org/https://doi.org/10.1016/j.engstruct.2022.114294.

[54] R. Ghanem, P. Spanos, Stochastic finite elements - A spectral approach, Springer Verlag, 1991.

[55] I. Sobol, Global sensitivity indices for nonlinear mathematical models and their Monte Carlo estimates, Math. Comput. Simul. 55 (2001) 271–280.

[56] B. Sudret, Global sensitivity analysis using polynomial chaos expansions, Reliab. Eng. Syst. Saf. 93 (2008) 964–979. https://doi.org/10.1016/j.ress.2007.04.002.

[57] M. Asali, Modélisation et prévision du comportement thermo-hydro-mécanique d'une paroi en béton : application au cas des enceintes de confinement des bâtiments réacteurs nucléaires, PhD thesis, Université Lille 1, 2016.

[58] G. Blatman, B. Sudret, Adaptive sparse polynomial chaos expansion based on least angle regression, J. Comput. Phys. 230 (2011) 2345–2367. https://doi.org/10.1016/j.jcp.2010.12.021.

[59] N. Lüthen, S. Marelli, B. Sudret, Sparse Polynomial Chaos Expansions: Literature Survey and Benchmark, SIAM/ASA, SIAM/ASA J. Uncertain. Quantif. 9 (2021) 593–649.

[60] M.D. McKay, R.J. Beckman, W.J. Conover, A Comparison of Three Methods for Selecting Values of Input Variables in the Analysis of Output from a Computer Code, Technometrics. 21 (1979) 239–245.

Declaration of interests

☒The authors declare that they have no known competing financial interests or personal relationships that could have appeared to influence the work reported in this paper.

☐The authors declare the following financial interests/personal relationships which may be considered as potential competing interests: